Monthly Notices of the ROYAL ASTRONOMICAL SOCIETY
MNRAS **508,** 2019–2038 (2021) https://doi.org/10.1093/mnras/stab2613

LeMMINGs III. The *e*-MERLIN legacy survey of the Palomar sample: exploring the origin of nuclear radio emission in active and inactive galaxies through the [O III] – radio connection

R. D. Baldi,[1,2★] D. R. A. Williams,[3] R. J. Beswick,[3] I. McHardy,[2] B. T. Dullo,[4] J. H. Knapen,[5,6] L. Zanisi,[2] M. K. Argo,[3,7] S. Aalto,[8] A. Alberdi,[9] W. A. Baan,[10] G. J. Bendo,[3,11] D. M. Fenech,[12] D. A. Green,[13] H.-R. Klöckner,[14] E. Körding,[15] T. J. Maccarone,[16] J. M. Marcaide,[17] I. Mutie,[3,18] F. Panessa,[19] M. A. Pérez-Torres,[9] C. Romero-Cañizales,[20] D. J. Saikia,[21] P. Saikia,[22] F. Shankar,[2] R. E. Spencer,[3] I. R. Stevens,[23] P. Uttley,[24] E. Brinks,[25] S. Corbel,[26,27] I. Martí-Vidal,[28] C. G. Mundell,[29] M. Pahari[30] and M. J. Ward[31]

Affiliations are listed at the end of the paper

Accepted 2021 September 7. Received 2021 September 5; in original form 2021 March 18

ABSTRACT

What determines the nuclear radio emission in local galaxies? To address this question, we combine optical [O III] line emission, robust black hole (BH) mass estimates, and high-resolution *e*-MERLIN 1.5-GHz data, from the LeMMINGs survey, of a statistically complete sample of 280 nearby optically active (LINER and Seyfert) and inactive [H II and absorption line galaxies (ALGs)] galaxies. Using [O III] luminosity ($L_{[\mathrm{O\,III}]}$) as a proxy for the accretion power, local galaxies follow distinct sequences in the optical–radio planes of BH activity, which suggest different origins of the nuclear radio emission for the optical classes. The 1.5-GHz radio luminosity of their parsec-scale cores (L_{core}) is found to scale with BH mass (M_{BH}) and [O III] luminosity. Below $M_{\mathrm{BH}} \sim 10^{6.5}$ M$_\odot$, stellar processes from non-jetted H II galaxies dominate with $L_{\mathrm{core}} \propto M_{\mathrm{BH}}^{0.61\pm0.33}$ and $L_{\mathrm{core}} \propto L_{[\mathrm{O\,III}]}^{0.79\pm0.30}$. Above $M_{\mathrm{BH}} \sim 10^{6.5}$ M$_\odot$, accretion-driven processes dominate with $L_{\mathrm{core}} \propto M_{\mathrm{BH}}^{1.5-1.65}$ and $L_{\mathrm{core}} \propto L_{[\mathrm{O\,III}]}^{0.99-1.31}$ for active galaxies: radio-quiet/loud LINERs, Seyferts, and jetted H II galaxies always display (although low) signatures of radio-emitting BH activity, with $L_{1.5\,\mathrm{GHz}} \gtrsim 10^{19.8}$ W Hz^{-1} and $M_{\mathrm{BH}} \gtrsim 10^{7}$ M$_\odot$, on a broad range of Eddington-scaled accretion rates ($\dot{m}$). Radio-quiet and radio-loud LINERs are powered by low-$\dot{m}$ discs launching sub-relativistic and relativistic jets, respectively. Low-power slow jets and disc/corona winds from moderately high to high-$\dot{m}$ discs account for the compact and edge-brightened jets of Seyferts, respectively. Jetted H II galaxies may host weakly active BHs. Fuel-starved BHs and recurrent activity account for ALG properties. In conclusion, specific accretion–ejection states of active BHs determine the radio production and the optical classification of local active galaxies.

Key words: galaxies: active – galaxies: jets – galaxies: nuclei – galaxies: star formation – radio continuum: galaxies.

1 INTRODUCTION

Supermassive black holes (SMBHs) are expected to reside at the centre of all massive galaxies (e.g. Aller & Richstone 2002; Marconi et al. 2004; Shankar et al. 2004). The accretion on to SMBHs in active galactic nuclei (AGN) provides a major power source in the Universe and is believed to regulate the evolution of galaxies by injecting energy and momentum ('feedback', Fabian 2012). Such feedback sets the reciprocal relation between the observed properties of SMBHs [e.g. central velocity dispersion σ as a proxy of black hole (BH) mass] and their host bulges (e.g. Magorrian et al. 1998; Gebhardt et al. 2000; Häring & Rix 2004). Much of our understanding of AGN phenomena (feeding and feedback) comes from the study of bright, powerful active SMBHs that have accreted primarily during typical active periods of the order of a few 10^8 yr in a radiatively efficient mode, as Seyfert nuclei and QSOs (Marconi et al. 2004; Shankar et al. 2004; Cao 2007). During such a phase, a geometrically thin, optically thick, standard accretion disc (SAD, Shakura & Sunyaev 1973), characterized by a high radiative efficiency mode (mass-to-energy conversion efficiency of $\epsilon \sim 0.1$, e.g. Shankar et al. 2020), is needed both to reproduce the currently observed SMBH space density and large-scale environment and to solve the Soltan argument (Soltan 1982).

However, the vast majority of SMBHs in the local Universe are in a quiescent state or, unless activity has been seen in some band, of extremely low nuclear outputs (e.g. Huchra & Burg 1992; Filho, Barthel & Ho 2006; Ho 2008): the latter are regarded to host a low-luminosity AGN (LLAGN, traditionally defined as having Hα luminosities $\leq 10^{40}$ erg s^{-1}; Ho, Filippenko & Sargent 1997a). Unfortunately, the weakness of the radiative signals from low-activity SMBHs makes their study difficult. Problems include: (i) confusion with brighter, non-AGN components, (ii) obscuration, and (iii) selection effects.

★ E-mail: ranieri.baldi@inaf.it

© 2021 The Author(s)
Published by Oxford University Press on behalf of Royal Astronomical Society

Downloaded from https://academic.oup.com/mnras/article/508/2/2019/6385009 by guest on 03 September 2022

The scarcity of deep multi-band studies for large samples of LLAGN means that understanding SMBH activity in the low-luminosity regime is currently limited. Theories indicate that LLAGN are characterized by a low accretion rate ($\dot{m}$) and/or low radiative efficiency (Ho 1999; Panessa et al. 2007). In models of radiatively inefficient accretion flows (RIAFs; Narayan & Yi 1994, 1995; Yuan, Bu & Wu 2012a; Yuan, Wu & Bu 2012b; White, Quataert & Gammie 2020), the kinetic energy is either advected with the gas into the SMBH or channelled into an outflow. The magnetic field combined with 'puffed-up' geometrically thick structures could provide a plausible mechanism for collimating axial outflows, accounting for a large fraction of observed jets in LLAGN (Maoz 2007; Mezcua & Prieto 2014).

Probably, the most common manifestation of LLAGN appears in the form of low-ionization nuclear emission-line regions (LINERs; Heckman 1980), which are detected in the nuclei of a large fraction of nearby galaxies (Ho, Filippenko & Sargent 1997b; Kauffmann et al. 2003). The current picture of LINERs is a 'mixed bag' of objects, with some photoionized by stars, some by AGN, and some perhaps excited by shocks (Allen et al. 2008; Sarzi et al. 2010; Capetti & Baldi 2011; Singh et al. 2013). By assuming an active BH origin of the LINER population (or a part of it), the transition from the Seyfert to LINER regime corresponds to a decrease in the Eddington ratio (defined as the ratio between the bolometric AGN luminosity and the Eddington luminosity, $L_{\rm Bol}/L_{\rm Edd}$) (Kewley et al. 2006; Ho 2008), accompanied by a hardening of the ionizing spectrum. At the extremely low end of the Eddington luminosity, active SMBHs with low $\dot{m}$ and low radiative efficiency can even be hidden at the centre of (apparently) inactive galaxies, where star formation (SF) outshines the faint active nucleus.

Understanding the physics of the accretion/ejection of matter in low-luminosity regimes is important for a variety of reasons. First, the steep local AGN luminosity function shows that LLAGN outnumber the QSO population by a few orders of magnitudes at $z < 0.3$ (Heckman & Best 2014; Saikia et al. 2018b). The large abundance of local LLAGN indicates that such a population represents the common mode of SMBH accretion at low redshifts and gives a snapshot of the ordinary relation between the SMBH and its host. Secondly, the identification of the LLAGN population would help to constrain the occupation fraction of active SMBH in galaxies. Such a quantity is unknown at low stellar masses $<10^{9-10}$ M$_\odot$ (Greene 2012; Gallo & Sesana 2019) and is crucial for establishing the BH mass density function and to calibrate the prescriptions for SMBH–galaxy growth of semi-analytical and numerical models (Shankar 2009; Barausse et al. 2017). Thirdly, the discovery of large cavities of hot gas that have been formed in the intracluster medium typically by jets from LLAGN in massive elliptical galaxies (e.g. Dunn & Fabian 2006; Werner et al. 2019) indicates that jet-mode feedback is a crucial aspect of the low-luminosity stage of SMBH activity (Heinz, Merloni & Schwab 2007; Fabian 2012).

In the last decades, the preferred method for finding active SMBHs was by X-ray selection, but even the deepest current observations cannot probe the heavily absorbed sources (e.g. the *Chandra* Deep Fields, Alexander et al. 2003). High-resolution radio observations [providing quantities such as, e.g. Spectral Energy Distribution (SED) or brightness temperature ($T_{\rm B}$)] offer complementary, direct views of BH accretion even in dusty environments and can detect AGN at $\dot{m}$ below those detectable in other wavebands.

In active galaxies, apart from stellar processes, a plethora of radio-emitting mechanisms associated with SMBH accretion can compete (see Panessa et al. 2019 for a review). Relativistic or sub-relativistic jets that accelerate particles (Padovani 2016; Blandford, Meier & Readhead 2019), disc winds that shock and sweep the interstellar medium (ISM) (Zakamska & Greene 2014), and outflowing magnetically active coronae (Laor & Behar 2008) are the main astrophysical phenomena that can account for cm/mm wavelength radiation in the pc-scale regions of AGN. The combination of radio and optical data can provide more robust diagnostics to separate SF and AGN components (see e.g. Best et al. 2005b; Kauffmann, Heckman & Best 2008; Smolčić et al. 2008; Best & Heckman 2012; Radcliffe et al. 2018; Muxlow et al. 2020) and break the degeneracy among all the possible radio-emitting physical processes: the goal of this work.

Jets,[1] generally seen in radio, but sometimes in other bands as well (e.g. in the optical, as in M 87, Perlman et al. 1999) are an unambiguous indicator of nuclear activity seen in LLAGN (e.g. Körding, Fender & Migliari 2006). The increasing evidence of finding jets associated with LLAGN compared to the high-luminosity AGN is supported by sparse radio studies of LLAGN and QSOs (e.g. Kukula et al. 1999; Nagar et al. 2000; Mezcua & Prieto 2014; Padovani 2016), although a few studies have found contradictory results (e.g. Jiang et al. 2007; Macfarlane et al. 2021). This result can be generalized by the fact that the radio loudness, i.e. the ratio between the radio and the optical emission associated with the active SMBH, increases at lower bolometric luminosities and at low Eddington ratios (Ho 2002, 2008; Kozieł-Wierzbowska et al. 2017; Laor, Baldi & Behar 2019). The presence of a link between the SMBH capability of emanating bright jets and their AGN multiband nuclear properties (bolometric luminosities, Eddington ratios, etc.) has been interpreted in the light of different accretion modes. Among active galaxies, RIAF discs and large SMBHs ($>10^8$ M$_\odot$) are generally more efficient at accelerating particles to relativistic velocities than SAD and small SMBHs (Meier 2001; Nemmen et al. 2007; Begelman 2012; McKinney, Tchekhovskoy & Blandford 2012). All these favourable conditions are generally met in LLAGN, which despite weak optical nuclei display a broad variety of radio properties from flat-spectrum cores to steep-spectrum kpc-scale jets (Nagar et al. 2000).

Since jets are observed across all types of active BHs [Galactic BHs, X-ray binaries (XRBs), and AGN], it is still under debate whether the accretion–jet symbiosis is scale-invariant, regardless of the accretion mode in, e.g. the so-called 'Fundamental Plane of BH activity' (Merloni, Heinz & di Matteo 2003; Falcke, Körding & Markoff 2004; Plotkin et al. 2012; Bonchi et al. 2013; Gültekin et al. 2019). This 3D plane (radio luminosity $L_{\rm radio}$, X-ray luminosity $L_{\rm X}$, and BH mass $M_{\rm BH}$) is believed to unify all active BHs at different mass scales, indicating common physical mechanisms in accretion and jet production among all accreting compact objects. Historically, in analogy with the states in XRBs, LINERs are thought to be the hard-state equivalent of an XRB, where the radiation is produced inefficiently and the jet is dominating over the disc emission ($L_{\rm X} \propto \dot{m}^2$, e.g. Esin, McClintock & Narayan 1997), while Seyfert galaxies are thought to be the equivalent of high-$\dot{m}$ XRBs ($L_{\rm X} \propto \dot{m}$, e.g. Fender, Gallo & Jonker 2003), where jets are never seen.[2] However, recently there is compelling evidence that the AGN optical classifications are not likely to map in a one-to-one manner to the spectral states observed from accreting stellar-mass BHs, and a

[1]The term 'jet' indicates outflow of ejected plasma that becomes collimated (unlike a wind), which transports outwards mass, energy, and angular momentum. The bulk speed can generally be relativistic, leading to a radio-loud AGN, or sub-relativistic, corresponding to a radio-quiet one.

[2]Dark decaying jets have been rarely seen in particular transitional stages of the soft state (e.g. Rushton et al. 2012; Drappeau et al. 2017).

Downloaded from https://academic.oup.com/mnras/article/508/2/2019/6385009 by guest on 03 September 2022

growing list of disc observational constraints of XRBs challenges its application to AGN (see review from Davis & Tchekhovskoy 2020). For AGN, the $\dot{m}$ break between LINERs and Seyferts is typically at about 10^{-3}, while for the XRBs hard states are typically seen below 2 per cent of $L_{\rm Edd}$ (Maccarone 2003; Vahdat Motlagh, Kalemci & Maccarone 2019), and soft states are typically seen above that level. A few Seyfert galaxies also show evidence of Fourier power spectra with similar characteristics to those of hard-state XRBs (Markowitz et al. 2003; Vaughan et al. 2005) and (low-luminosity) Seyferts often show jetted structures (e.g. Kukula et al. 1995; Thean et al. 2000; Giroletti & Panessa 2009; Kharb et al. 2017), differently from soft-state XRBs.

To have a less biased view of the properties of SMBH accretion and the SMBH–host link at low masses, an accurate census of the accretion and jet properties is needed. This requirement is satisfied by the LeMMINGs (Legacy *e*-MERLIN Multiband Imaging of Nearby Galaxy Sample) survey[3] (Beswick et al. 2014). It consists of 1.5-GHz observations (and upcoming 5-GHz observations) of 280 nearby galaxies from the Palomar sample, which is usually considered to be one of the best selected and most complete samples of nearby galaxies. The two data releases (Baldi et al. 2018, Paper I, and Baldi et al. 2021, Paper II) represent the deepest 1.5-GHz survey of local (<110 Mpc) active and inactive galaxies at milliarcsecond resolution and μJy sensitivity with the *e*-MERLIN array. Only partial conclusions on the optical–radio connection have been already drawn in Paper I because of incompleteness of the sample. The full coverage of the [O III]-line optical and radio data in this work allows to exploit the statistical completeness of the sample to investigate the origin of the radio cores in local galaxies.

In Section 2, we present the LeMMINGs project and the radio and optical [O III] properties of the sample. We show the optical–radio diagnostics to explore the nature of the radio emission for each optical class in Section 3. In Section 4, we discuss the results and focus on each optical class. We revise the radio properties of the LLAGN population and draw our conclusions about disc–jet coupling in LLAGN and SMBH-host connection in nearby galaxies in Section 5. A supplementary Section A focuses on the BH mass function of local galaxies.

2 THE SURVEY AND THE SAMPLE

The LeMMINGs sample represents a subset of 280 galaxies from the Revised Shapley-Ames Catalog of Bright Galaxies and the Second Reference Catalogue of Bright Galaxies (Sandage & Tammann 1981) (details in Papers I and II). The sample is taken from the optical spectroscopic Palomar survey (Ho et al. 1997a), selecting only targets with $\delta > 20^{\circ}$, to be accessible to the *e*-MERLIN array. The sample is optically selected ($B_{\rm T} < 12.5$ mag) and so has no radio bias and a median distance of 20 Mpc. Based on the updated optical emission-line diagnostic diagrams (BPT, Baldwin, Phillips & Terlevich 1981; Kewley et al. 2006; Buttiglione et al. 2010), the sample has been classified into H II, Seyfert, LINER, and absorption line galaxies (ALGs) (see Papers I and II). The galaxies for which the active SMBH is the main photoionizing source are Seyferts (18/280) and LINERs (94/280). The inactive galaxies are represented by H II galaxies (140/280) where star-forming regions populated by massive young stars mainly photoionize the surrounding gas, and ALG (28/280), which are optically inactive galaxies and do not show evident emission lines and are typically in early-type hosts.

[3]http://www.e-MERLIN.ac.uk/legacy/projects/lemmings.html

e-MERLIN observations at *L*-band (1.2–1.7 GHz) of the 280 Palomar galaxies are presented in Papers I and II. An angular resolution of $\lesssim$200 mas and high sensitivity ($1\sigma \sim 0.8$ mJy beam^{-1}) enabled the detection of radio emission at pc scale of 44.6 per cent (125/280) of the sample. We detected the radio cores[4] with typical radio sizes of $\lesssim$100 pc and radio-core luminosities, $L_{\rm core}$, in the range $\sim 10^{34}$–10^{40} erg s^{-1} (Table 1). For 106 of the 125 detected sources, we identified the radio core within the structure, co-spatial with the optical galaxy centre: 56/94 LINERs, 12/18 Seyferts, 5/28 ALGs, and 33/140 H II galaxies. Conversely for the remaining 19 'unidentified' sources, the detected radio emission was not associated with the central optical nucleus. We resolved parsec-scale radio structures with a broad variety of morphologies (Table 1): core/core-jet (class A, the most common), one-sided jet (class B), triple sources (class C), double-lobed (class D), and complex shapes (class E) with extents of $\sim$3–6600 pc. There are 31 sources with clear jets (classes B, C, and D), which are referred to as 'jetted' galaxies. LINERs and Seyferts are the most luminous sources, whereas H II galaxies are the least. LINERs show elongated core-brightened radio structures while Seyferts reveal the highest fraction of symmetric morphologies. The majority of the 33 radio-detected H II galaxies have single radio core or complex extended structures, but seven of them show clear jets. ALGs exhibit on average the most luminous radio structures, similar to that of LINERs.

When considering the galaxy morphological types, most of the sources are late-type galaxies (LTGs, from Sa to Sd, $\sim$71 per cent), with a smaller fraction of elliptical and lenticulars (E and S0, early-type galaxies [ETGs]). In terms of BH masses, we derive the values using the stellar velocity dispersions σ measured from optical spectra (mostly from Ho et al. 2009, see Table 1) and the empirical $M_{\rm BH}$–σ relation from Tremaine et al. (2002), analogous to what was done in Paper I. For 36 sources, we use direct SMBH measurements (derived from stellar and gas dynamics, mega-masers, or reverberation mapping) available from the $M_{\rm BH}$ compilation of van den Bosch (2016). Our sample of 280 galaxies harbours BHs with $10^4 \lesssim M_{\rm BH} \lesssim 10^9$ M$_{\odot}$. As a test, we also derive the BH masses using the $M_{\rm BH}$–σ relation from van den Bosch (2016), which is based on a larger sample of BH masses than the one from Tremaine et al. (2002). The two relations agree with each other within 0.3 dex for intermediate BH masses, $\sim 10^6$–10^8 M$_{\odot}$, but differ at higher BH masses within 0.5 dex and at lower BH masses within 1 dex. This scatter defines the errors on the $M_{\rm BH}$ measurements. LINERs, Seyferts, and ALGs typically host SMBHs with masses $\gtrsim 10^7$ M$_{\odot}$, while H II galaxies have typically lower BH masses.

2.1 [O III] emission line

The [O III] emission line is an optical forbidden λ5007 Å transition, produced by gas photoionization by a strong radiation field from either an active SMBH or a star-forming region. In the case of an AGN, because of its high-energy ionization level, [O III] emission is extended from several kpc on galaxy scale down to the innermost central region on pc scale in the so-called 'narrow-line region' (NLR) (Kewley, Nicholls & Sutherland 2019). Despite being slightly dependent on the AGN orientation and obscuration (e.g. Risaliti, Salvati & Marconi 2011; Bisogni, Marconi & Risaliti 2017), [O III] line luminosity, $L_{\rm [O\,iii]}$, is a good (but not ideal) indicator of the

[4]We define core as the unresolved central component of the radio source, which pinpoints the location of a putative SMBH, and may represent a jet base, an unresolved disc-driven emission, or a nuclear stellar cluster (NSC).

Downloaded from https://academic.oup.com/mnras/article/508/2/2019/6385009 by guest on 03 September 2022

Table 1. Radio and optical properties of the LeMMINGs (Palomar) sample.

Name	Hubble	Class BPT	σ km s^{-1}	log M_{BH} M$_\odot$	log $L_{[O\,III]}$ erg s^{-1}	log Edd ratio	Det	Morph	log L_{core} erg s^{-1}	log L_{Total} erg s^{-1}
(1)	(2)	(3)	(4)	(5)	(6)	(7)	(8)	(9)	(10)	(11)
NGC 7817	SAbc	H	66.7	6.21	39.29	−1.51	U	–	<35.64	–
IC 10	IBm?	H	35.5	5.11	37.13	−2.57	U	–	<32.91	–
NGC 147	dE5 pec	ALG	22	4.28	–	–	U	–	<32.39	–
NGC 185	dE3 pec	L	19.9	4.10	34.63	−4.06	U	–	<32.33	–
NGC 205	dE5 pec	ALG	23.3	4.34*	–	–	U	–	<32.36	–

Note. Column description: (1) source name; (2) morphological galaxy type taken from RC3 (de Vaucouleurs et al. 1991); (3) optical spectroscopic classification based on BPT diagrams and from the literature. H = H II, S = Seyfert, L = LINER, and ALG = absorption line galaxy. 'j H' marks the jetted H II galaxies and 'RL' identifies the RL AGN; (4) stellar velocity dispersion σ (km s^{-1}) from Ho et al. (2009); (5) logarithm of BH mass ($M_\odot$) determined from σ (Tremaine et al. 2002) or from direct BH mass measurements (galaxies marked with *, van den Bosch 2016); (6) logarithm of [O III] luminosities from Ho et al. (1997a) or from the literature (non-corrected for extinction, see Paper II for references); (7) logarithm of Eddington ratio (L_{Bol}/L_{Edd}); (8) radio detection status: 'I' = detected and core identified; 'U' = undetected; 'unI' = detected but core unidentified; 'I + unI' = detected and core identified with additional unknown source(s) in the field; (9) radio morphological classes: A = core/core–jet; B = one-sided jet; C = triple; D = doubled-lobed; E = complex; (10)–(11) logarithm of radio core and total luminosities at 1.5 GHz (erg s^{-1}). To convert the radio luminosities in erg s^{-1} to W Hz^{-1} at 1.5 GHz, an amount of + 16.18 should be subtracted from log L_{core} and log L_{Total}. The full table is available as supplementary material.

bolometric AGN luminosity ($L_{Bol} = 3500 \times L_{[O\,iii]}$, Heckman et al. 2004 for LLAGN). Since the line emitting region can extend up to several kpc, the main caveat of the [O III] line is the contribution from other ionizing sources, such as shocks and purely stellar processes (Binette et al. 1994; Dickson et al. 1995; Dopita et al. 1997), which could result in an overestimate of the SMBH accretion power. Conversely, if the kpc-scale NLR extends beyond the spectroscopic slit used by Ho, Filippenko & Sargent (1995) (1–2 arcsec, from a few pc to ∼1 kpc for our sample), this may lead to an underestimate of the AGN bolometric luminosity.

For the LeMMINGs sample, we collect the [O III] luminosities (Table 1, not corrected for extinction) from the Palomar optical survey (Ho et al. 1997a) and from the most recent surveys/observations (see Papers I and II for more details). In our sample, Seyferts, LINERs, and H II galaxies have mean [O III] luminosities of 5.0×10^{39}, 3.5×10^{38}, and 1.5×10^{38} erg s^{-1}, respectively. For the vast majority of ALGs, upper limits on [O III] luminosities are not available.

Despite some caveats on $L_{[O\,iii]}$ as an indicator of AGN strength (e.g. Lamastra et al. 2009; Netzer 2009, particularly at low luminosities), we can also calculate the Eddington ratio, L_{Bol}/L_{Edd}, a gauge of the accretion rate, $\dot{m}$ (listed in Table 1 and shown in Fig. 1 for our sample). The Eddington ratios of LINERs and Seyferts are generally below and above 10^{-3}, respectively, the typical threshold used to separate between low and high $\dot{m}$ on to the SMBHs (Best & Heckman 2012). For H II galaxies, in the conservative scenario that their line emission is powered by the AGN, we note that, although less luminous in line emission, they have intermediate Eddington ratios between LINERs and Seyferts because their BH masses are typically lower than those of active galaxies.

Since optical emission lines (e.g. H α and [O III]) can be caused by hot, young massive stars in star-forming regions, we can also assume a stellar origin of the line emission: $L_{[O\,iii]}$ can thus be used as an SF rate (SFR) estimator, SFR (M$_\odot$/yr) $= 7.9 \times 10^{-42}\, L_{[O\,iii]}$ (erg s^{-1}) following Kennicutt (1998) and adopting log([O III]/H α) $= 0.0 \pm 0.5$ (Moustakas, Kennicutt & Tremonti 2006; Suzuki et al. 2016).

2.2 Radio loudness

The investigation of the nature of the radio emission in the LeMMINGs galaxies would benefit from a separation between radio-loud (RL) and radio-quiet (RQ) AGN. For the former (i.e. radio galaxies, RGs), the relativistic jets are the main power source; for the latter, different mechanisms (SF, sub-relativistic jets, and disc/corona winds) are likely to produce radio continuum (Panessa et al. 2019). Accordingly, we have used the ratio $L_{core}/L_{[O\,iii]}$ defined as the spectroscopic radio-loudness parameter (Capetti & Balmaverde 2006) based on local ellipticals. In general, Seyfert galaxies and RQ AGN show a larger excess of line emission (at a given radio-core luminosity) than those of RL objects, i.e. $L_{radio}/L_{[O\,iii]} < 10^{-2}$ (Capetti & Balmaverde 2007; Ishibashi et al. 2014). Since the LeMMINGs sample contains a more heterogeneous mixture of early- and late-type galaxies than the sample used by Capetti & Balmaverde (2006), and RL AGN are known to be associated with the most massive BHs[5] (Chiaberge & Marconi 2011), we select the RL galaxies (black circles, Fig. 2) based on these two

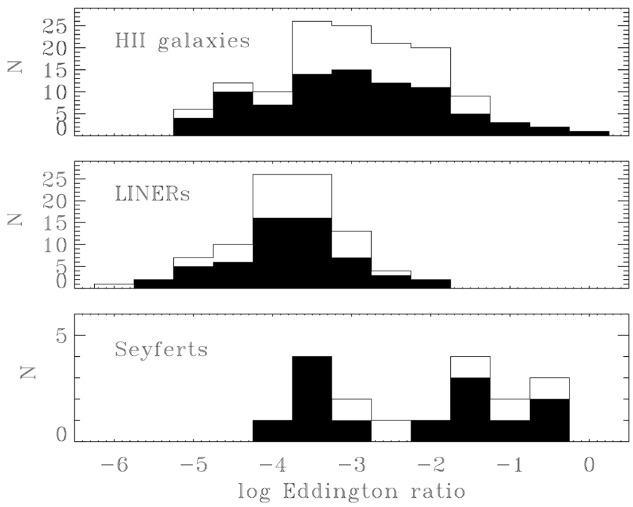

Figure 1. The Eddington ratio (ratio between the bolometric AGN luminosity, $L_{Bol} = 3500 \times L_{[O\,iii]}$, Heckman et al. 2004 for LLAGN and the Eddington luminosity) for the LeMMINGs sample with the [O III] line detected: H II, LINER, and Seyfert galaxies. The filled histogram identifies the radio-detected sources.

[5]More than 80 per cent of the local AGN with $M_{BH} > 10^{7.7}$ M$_\odot$ and with 150-MHz radio luminosities $>10^{21}$ W Hz^{-1} are RL (Sabater et al. 2019).

Downloaded from https://academic.oup.com/mnras/article/508/2/2019/6385009 by guest on 03 September 2022

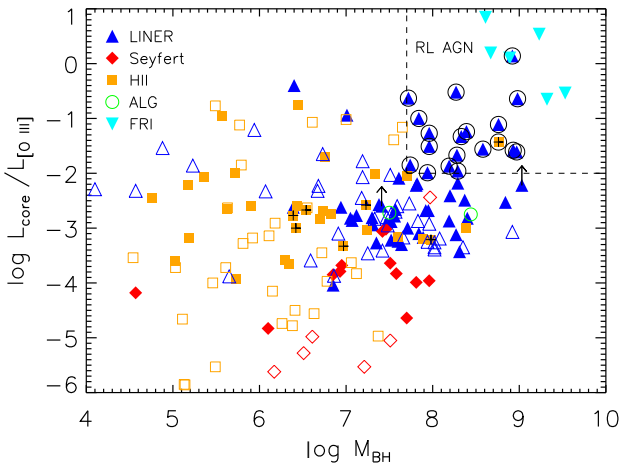

Figure 2. The spectroscopic radio-loudness parameter $L_{\rm core}/L_{\rm [O\,III]}$ as a function of $M_{\rm BH}$ (in $M_\odot$) for our sample. The area limited by the dashed line encloses the RL AGN (black circles), selected to have $L_{\rm core}/L_{\rm [O\,III]} > 10^{-2}$ and $M_{\rm BH} > 10^{7.7}$ $M_\odot$. The symbols and colour codes are described in the legend: LINERs as blue up-pointing triangles, Seyferts as red diamonds, and H II galaxies as orange squares. The filled (empty) symbols are the radio-detected (non-detected with 3σ upper limits) radio sources. The plus signs identify the jetted H II galaxies. We also include six 3C/FR Is (pale-blue down-pointing triangles) to highlight the locus of RL AGN.

conditions: $L_{\rm core}/L_{\rm [O\,III]} > 10^{-2}$ and $M_{\rm BH} > 10^{7.7}$ $M_\odot$ (in agreement with local RL LLAGN, Baldi & Capetti 2010). The selected RL AGN in the LeMMINGs sample are thus 18 LINERs and one jetted H II galaxy (see Table 1).

The radio loudness is known to increase with $M_{\rm BH}$ (Fig. 2, see Nelson 2000; Best et al. 2005b), and the presence of a bimodal, dichotomous, or continuous distribution of radio loudness between RQ and RL AGN is still controversial (e.g. Kellermann et al. 1989; Cirasuolo et al. 2003). In fact, we note that other possible RL candidates (mostly LINERs) are close to our RL/RQ selection boundary. A clean RQ/RL separation simply based on the radio-loudness parameter and BH mass is not possible, as a detailed radio study of the jet with very-long baseline interferometers (VLBI) would be needed (see Giovannini 2003, 2004). Therefore, our criteria select the most bona fide RL AGN of the sample. Furthermore, the radio loudness is also known to inversely correlate with the Eddington ratio (Ho 2008; Yang et al. 2020). However, since in our case both quantities are derived from the [O III] luminosities (i.e. the spectroscopic radio loudness $\propto L^{-1}_{\rm [O\,III]}$ and Eddington ratio $\propto L_{\rm [O\,III]}$), an inverse correlation between these two quantities is hence expected.

3 THE OPTICAL–RADIO CONNECTION AND THE ORIGIN OF THE RADIO EMISSION

BPT diagrams attribute the optical emission lines of LINERs and Seyferts to photoionization from AGN activity, whereas for H II galaxies the line ionization is most likely due to SF processes. The paucity of studies on the nuclear emission of ALGs casts doubts on the nature of this class of sources. However, the origin of the radio emission associated with an optical nucleus for each class is controversial, since several processes compete (Panessa et al. 2019). The [O III] line emission taken from the Palomar spectroscopic survey is extracted from a more extended nuclear region than the sub-arcsec radio emission detected by our *e*-MERLIN survey. A direct spatial comparison between the optical and radio-emitting regions is therefore not possible in this work. Consequently, a possible mismatch between the spatial distributions of the radio and optical regions could lead to a misinterpretation of the origin of the radio emission, e.g. genuine AGN-driven nucleus in an H II galaxy. Fortunately, forthcoming studies with integral-field spectroscopy (e.g. from the MaNGA survey, Bundy et al. 2015) on local radio-emitting galaxies (e.g. Roy et al. 2021; Mulcahey 2021) and with *HST* photometry on the LeMMINGs sample itself (Dullo et al. 2021 will clarify this point.

In analogy to Paper I for a sub-sample (103 objects), we here carefully study the connection between the radio emission down to ∼50 pc and the sub-kpc [O III] emission, weighing the role of $M_{\rm BH}$, for the entire LeMMINGs sample. Specifically, we explore the $L_{\rm core}$–$L_{\rm [O\,III]}$–$M_{\rm BH}$ relation to investigate the origin of nuclear radio emission in active and inactive galaxies.

3.1 Radio properties versus BH mass

Hints to possibly identify the genuine AGN origin of the nuclear emission come from two quantities: the BH mass and the radio luminosity. The former is often used as an indicator of BH activity as active nuclei are preferentially associated with massive systems (e.g. Chiaberge & Marconi 2011). The latter roughly establishes the likelihood of the source being radio-jet dominated, a sign of an active SMBH (Cattaneo & Best 2009). Both quantities are connected in active nuclei, as AGN tend to become more radio powerful (e.g. radio louder) at larger $M_{\rm BH}$ (e.g. Best et al. 2005b).

The distribution of radio-detected galaxies as a function of BH mass in the LeMMINGs sample is shown in Fig. 3 (upper panel) and it is clear that the detection fraction increases with $M_{\rm BH}$ (a closer look in Fig. 4). Similarly, a positive trend between the radio-core luminosities, $L_{\rm core}$, and $M_{\rm BH}$ is also observed (lower panel, Fig. 3). In analogy to Paper I, for the objects with $M_{\rm BH} \gtrsim 10^{6.5}$ $M_\odot$, a clear sequence includes all active and jetted galaxies, despite the large scatter. However, below $10^{6.5}$ $M_\odot$, which mostly includes H II galaxies, a flatter correlation emerges. Interestingly, the small sub-group of jetted H II galaxies has $M_{\rm BH} \gtrsim 10^{6.5}$ $M_\odot$ and generally follows the sequence of the active galaxies.

In order to assess the presence of correlations, we performed a statistical censored analysis (ASURV package; Feigelson & Nelson 1985; Lavalley, Isobe & Feigelson 1992), which takes into account upper limits. We used the `schmittbin` task (Schmitt 1985) to calculate the associated linear regression coefficients for two sets of variables. The best fit is represented by the bisector of the two regression lines obtained by switching the *x*- and *y*-axes as dependent and independent variables. In order to estimate the quality of the linear regression, for small data sets ($N < 30$) we also derived the generalized Kendall's τ correlation coefficient (Kendall 1938) between the two variables, using the bhkmethod task. Otherwise for larger samples, we used the Spearman's rank order correlation coefficient, using the spearman task (Akritas 1989). To measure the linear correlation between two fully detected sets of data, we estimate the Pearson correlation coefficient r (Pearson 1895). We also test the possible influence of the sample distance D in driving the established correlations, estimating the censored partial rank coefficient $\rho_{\rm XY,\,D}$ (Akritas & Siebert 1996). Table 2 reports the parameters of the statistical analysis of the correlations we analyze hereafter in this work.

We fit the linear (in a log–log plot, hereafter) radio–$M_{\rm BH}$ correlation by including all the active galaxies, i.e. those that show characteristics of AGN activity in optical (emission line ratios) or radio (presence of jets) bands: RQ/RL LINERs, Seyferts, and

Downloaded from https://academic.oup.com/mnras/article/508/2/2019/6385009 by guest on 03 September 2022

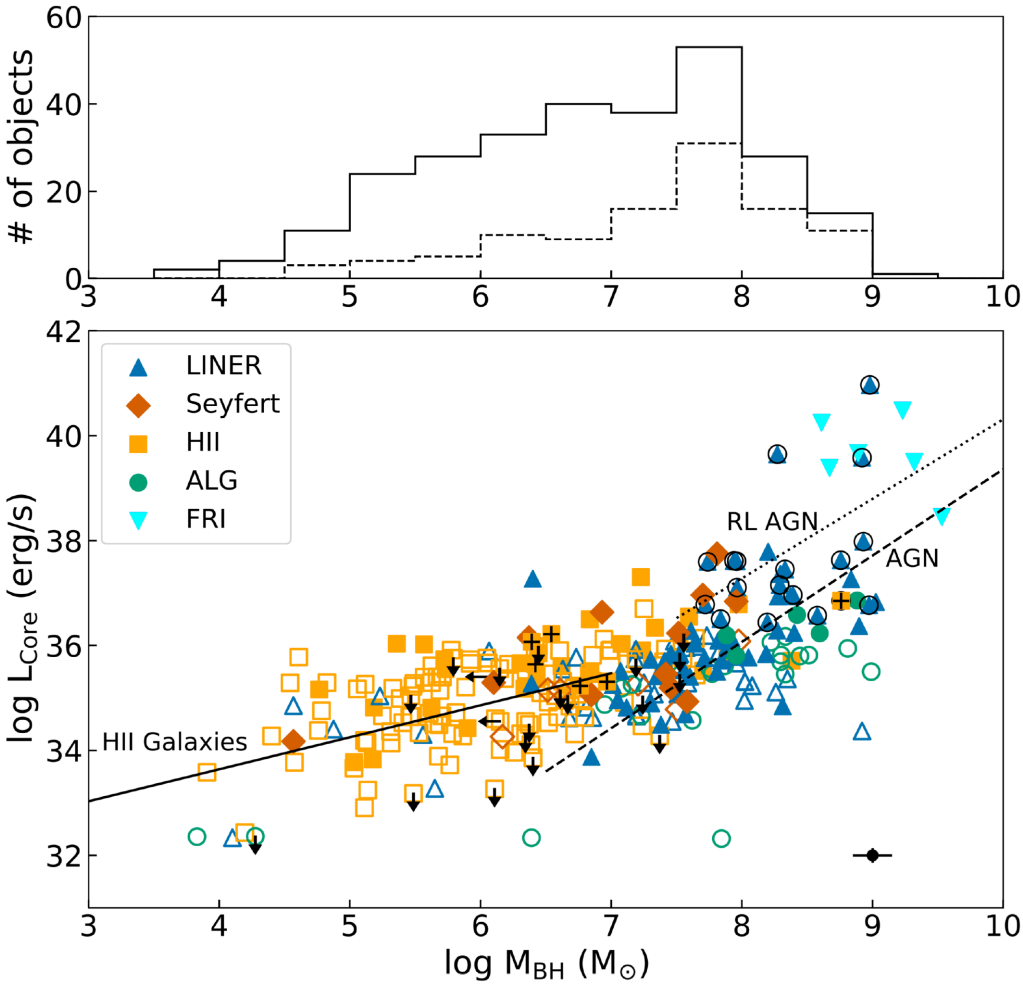

Figure 3. In the upper plot, the histograms of the entire sample (solid line) and of radio-detected sources (dashed line) in bins of BH mass. In the lower panel, 1.5-GHz core luminosities ($L_{\rm core}$ in erg s^{-1}) as a function of the BH masses (in M$_\odot$) for the sample, divided per optical class (symbol and colour coded as in the legend, analogous to Fig. 2). The filled symbols refer to the detected radio sources, while the empty symbols refer to non-detected radio sources (3σ upper limits). The unidentified sources (detected but the radio core has not been identified) are the empty symbols with radio 3σ upper limits. The jetted H II galaxies show an additional plus sign. The dotted line represents the linear correlation found for RL AGN (marked by black circles) and 3C/FR Is, the dashed line for active and jetted (ALG and H II) galaxies for $M_{\rm BH} \gtrsim 10^{6.5}$ M$_\odot$, and the solid line for the non-jetted H II galaxies for $M_{\rm BH} \lesssim 10^{6.5}$ M$_\odot$ (see Section 3.1 for details and Table 2 for the best-fitting parameters using censored-data statistics). In the bottom right corner, we show the typical error bars associated with the data points.

jetted ALG and H II galaxies. For BH masses $\gtrsim 10^{6.5}$ M$_\odot$, we find $L_{\rm core} \propto M_{\rm BH}^{1.65\pm0.25}$ with a Spearman's correlation coefficient of 0.549. This value shows the likelihood of the two quantities not correlating as less than 1×10^{-4} (Table 2).

In contrast, the non-jetted H II galaxies tend to fall on another radio–$M_{\rm BH}$ sequence with $M_{\rm BH} \lesssim 10^{6.5}$ M$_\odot$. Indeed, their relation clearly flattens with respect to that of active galaxies as $L_{\rm core} \propto M_{\rm BH}^{0.61\pm0.33}$ with a chance (Spearman's $\rho = 0.575$) probability of correlation of 3×10^{-4} (Table 2). The two incident radio–$M_{\rm BH}$ relations valid for star-forming and active galaxies strengthen the scenario of a different origin of the radio emission: SF-driven for non-jetted H II galaxies and AGN-driven for active galaxies.

Paper I suggested that LINERs and low-power RGs are powered by a common central engine, e.g. a RIAF disc with a coupled jet (Falcke et al. 2004; Nemmen, Storchi-Bergmann & Eracleous 2014). Paper I compiled a sample of six Fanaroff & Riley type I (FR I) RGs (i.e. 3C 66B, 3C 264, 3C 78, 3C 338, 3C 274, and 3C 189, from the Revised Third Cambridge Catalogue, 3C, Bennett 1962) at z <0.05 observed with MERLIN at 1.5 GHz (see table 4 in Paper I). In Figs 2 and 3, FR Is stand out from the rest of the sources for their large radio luminosities and BH masses, and thus higher radio loudness, and clearly extend the LINER population to higher values. Therefore, we fit the mass–radio relation valid for the whole RL AGN group (RL Palomar + FR I galaxies, dotted line in Fig. 3). We find $L_{\rm core} \propto M_{\rm BH}^{1.52\pm0.31}$ with a Pearson correlation coefficient of 0.526 and a two-sided no-correlation probability significance of 6.9×10^{-4}.

Two different radio-$M_{\rm BH}$ sequences below and above $\sim 10^{6.5}$ M$_\odot$, respectively, for star-forming and active galaxies have been thus validated also by excluding the distance effect in driving the correlations (as the censored partial rank coefficients only marginally decrease, see Table 2). Therefore, now that the presence of a break at $M_{\rm BH} \sim 10^{6.5}$ M$_\odot$ has been highlighted, we can focus on the fraction of radio detections, $f_{\rm d}$, as a function of $M_{\rm BH}$ for the entire LeMMINGs sample (Fig. 4). For $M_{\rm BH} > 10^{7.5}$ M$_\odot$, this fraction is 50 per cent, reaching >75 per cent in the last bins, $>10^{8.5}$ M$_\odot$. Conversely, the fraction flattens at ∼20 per cent below $\sim 10^{6.5}$ M$_\odot$, where the SF was

Downloaded from https://academic.oup.com/mnras/article/508/2/2019/6385009 by guest on 03 September 2022

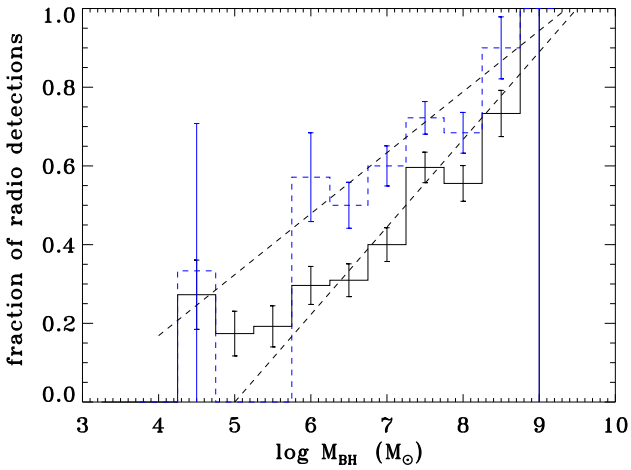

Figure 4. Histograms of the fraction of radio-detected galaxies in the LeMMINGs sample in M_{BH} bins. The solid-line histogram considers the entire sample, while the blue dashed line is the distribution of only the active galaxies (LINER, Seyferts, and jetted ALG and H II galaxies). The two dashed lines represent the best fit for two distributions (Table 2 for the best-fitting parameters).

found to largely contribute in our sample (Fig. 3). By considering only the sub-sample of active galaxies, the fraction of radio detections is unexpectedly higher than that of the entire sample in each BH mass bin. We also note that the f_d reaches 100 per cent for active galaxies with $L_{core} \gtrsim 10^{36}$ erg s^{-1} ($\gtrsim 10^{19.8}$ W Hz^{-1}) and $M_{BH} \gtrsim 10^7$ M$_\odot$. We fit the two detection fraction distributions as a function of BH mass for $M_{BH} > 10^{6.5}$ M$_\odot$ to avoid both the SF flattening and a single AGN case (Seyfert NGC 4395[6]). The best fits (see statistical parameters in Table 2) are $f_d \propto M_{BH}^{0.22\pm0.03}$ and $\propto M_{BH}^{0.15\pm0.03}$, respectively, for the whole LeMMINGs sample and for the active galaxies.

All of the radio morphological classes are represented along the radio (both L_{core} and f_d) $-$ M_{BH} sequence. The total integrated radio luminosity, L_{Total}, also broadly increases with the BH mass (Fig. 5). There is no overall trend that links a specific radio morphological classification to a given range of radio luminosities. The fraction of targets assigned to classes B, C, D, and E (e.g. clear jetted structures or complex) typically increases with L_{Total}/M_{BH} because of their large extended, and sometimes diffuse, radio emission. Core/core–jet structures (class A) are observed across a slightly broader M_{BH} and L_{Total} range than the other classes. A similar effect has been also noted in the L_{core}–M_{BH} plot. This could be the consequence of two effects: the preference for faint sources to appear as single cores and a Doppler-boosted flux in the case of aligned sources. However, the latter scenario, i.e. a core boosting, is expected to marginally affect our results at 1.5 GHz in the sub-mJy regime (only for RL AGN, see e.g. blazar-like heart of NGC 1275, Walker, Romney & Benson 1994).

3.2 Radio properties versus [O III] luminosity

The comparison between radio and optical properties of galaxies is a powerful tool to explore the nature of their nuclear emission. The [O III] luminosity represents a robust upper limit (unless there is strong dust extinction) to any bolometric emission from an accretion disc in the case of an AGN (Lamastra et al. 2009) (or from stellar emission in the case of an H II galaxy, Moustakas et al. 2006). The radio emission efficiency, i.e. the fraction of the radio emission produced with respect to the AGN (or SF) bolometric luminosity, offers a good diagnostic to investigate the nature of the nuclei.

The radio-core luminosity as a function of [O III] luminosity is shown in Fig. 6 for the LeMMINGs sample (without ALGs that lack optical counterparts but including NGC 5982 with an $L_{[O\,iii]}$ upper limit). The three optical classifications (LINER, Seyfert, and HII galaxy) tend to cluster in different regions of the [O III]–radio diagram, despite a large overlap, similar to what has been noted in the analogous plot for a smaller sub-sample in Paper I. Seyferts are up to 100 times more luminous in the [O III] emission line compared with LINERs for a given L_{core} or equivalently have 100 times less luminous radio cores. The H II galaxies have the lowest radio and [O III] luminosities, while the LINERs have intermediate values. Analogously to Paper I, we report that the LINERs appear to broadly follow a linear trend in the [O III]-radio plot. Similar to Fig. 3, the relation formed by H II galaxies shows a break with respect to that valid for active galaxies at lower luminosities. Compared to the results from Paper I, we note that Seyferts show a distinct relation with respect to the other classes. The current complete sample allows us to derive more robust relations by using the censored data analysis (see Table 2) than those obtained in Paper I.

First, Seyfert galaxies clearly show a striking linear correlation in the form $L_{core} \propto L_{[O\,iii]}{}^{0.99\pm0.20}$ with a (Kendall's $\rho = 1.190$) probability of 0.0002 of being caused fortuitously. At higher radio luminosities, RL AGN follow the 3C/FR Is on a steeper linear fit, $L_{core} \propto L_{[O\,iii]}{}^{1.31\pm0.18}$ (Pearson's P value $= 9.4 \times 10^{-9}$). RQ LINERs fill the gap between RL AGN and Seyferts with a correlation almost parallel to the one found for RGs, i.e. $L_{core} \propto L_{[O\,iii]}{}^{1.21\pm0.28}$ (Spearman's P value <0.0001). At low powers, the sequence of non-jetted H II galaxies clearly flattens with respect to that formed by active galaxies but with a broader scatter, i.e. $L_{[O\,iii]} \propto L_{core}{}^{0.79\pm0.30}$ (Spearman's P value <0.0001). Once the distance dependence has been considered, these optical–radio relations are still statistically valid, because the censored partial rank coefficients are only slightly smaller than the generalized correlation coefficients (see Table 2).

Beyond the optical classification, the sources with a core/core–jet or triple structure tend to follow the correlation of the active galaxies, as they are mostly classified as LINERs and Seyferts. Similarly, most of the ETGs also follow the correlation of active galaxies. Conversely, we do not find any statistically significant correlation between the Eddington ratios and L_{core} for our sample (see Fig. 7, probability of fortuitous correlations >0.04). Nevertheless, we note for Seyferts: (i) a mild positive trend where L_{core} and Eddington ratio linearly increases with a slope 0.98 ± 0.36 with a large scatter ~1 dex [Kendall's $\rho = 0.591$ (essentially unchanged correlation coefficient, if considering the distance dependence] and probability of a null correlation 0.0149, Table 2)] and (ii) the jetted morphologies correspond to objects with higher Eddington rates.

3.3 The optical fundamental plane of BH activity

Observational attempts at explaining the similarities between the X-ray and radio properties of SMBHs and XRBs eventually culminated in the discovery of the so-called 'Fundamental Plane of Black Hole Activity' (hereafter 'FPBHA', Heinz & Sunyaev 2003; Merloni et al. 2003; Falcke et al. 2004). The FPBHA is a 3D hyper-plane that correlates the radio luminosity with the X-ray luminosity, scaled by the BH mass, and seems to hold for XRBs and active SMBHs. By using a similar approach, Saikia, Körding & Falcke (2015) introduced a new version of the FPBHA using the [O III] luminosity as a tracer of

[6]The active galaxy with the lowest M_{BH} of the sample, 3.7×10^4 M$_\odot$.

Downloaded from https://academic.oup.com/mnras/article/508/2/2019/6385009 by guest on 03 September 2022

Table 2. Statistical censored analysis of radio-optical correlations of the full LeMMINGs sample presented as a function of galaxy type.

X (1)	Y (2)	Fig. (3)	Sub-sample (4)	Stat (5)	ρ_{XY} (6)	$P_{\rho_{XY}}$ (7)	$\rho_{XY,D}$ (8)	Slope (9)	Intercept (10)
$\log M_{\rm BH}$	$\log L_{\rm core}$	3	Active galaxies	S	0.549	<0.0001	0.526	1.65 ± 0.25	23.0 ± 8.1
$\log M_{\rm BH}$	$\log L_{\rm core}$	3	Non-jetted H II	S	0.575	0.0003	0.541	0.61 ± 0.33	31.2 ± 8.7
$\log M_{\rm BH}$	$\log L_{\rm core}$	3	RL AGN + 3C/FR I	P	0.526	0.00069	0.496	1.52 ± 0.31	25.1 ± 4.1
$\log M_{\rm BH}$	$f_{\rm d}$	4	All ($M_{\rm BH} > 10^{6.5}$ M$_\odot$)	P	0.951	0.00098	–	0.22 ± 0.03	-1.11 ± 0.24
$\log M_{\rm BH}$	$f_{\rm d}$	4	Active gal. ($M_{\rm BH} > 10^{6.5}$ M$_\odot$)	P	0.925	0.0028	–	0.15 ± 0.03	-0.45 ± 0.21
$\log L_{\rm [O\,iii]}$	$\log L_{\rm core}$	6	Seyferts	K	1.190	0.0002	0.920	0.99 ± 0.20	-3.5 ± 5.5
$\log L_{\rm [O\,iii]}$	$\log L_{\rm core}$	6	RL AGN + 3C/FR I	P	0.876	9.4×10^{-9}	0.840	1.31 ± 0.18	-13.1 ± 7.0
$\log L_{\rm [O\,iii]}$	$\log L_{\rm core}$	6	RQ LINERs	S	0.579	<0.0001	0.542	1.21 ± 0.28	-11.1 ± 6.4
$\log L_{\rm [O\,iii]}$	$\log L_{\rm core}$	6	Non-jetted H II	S	0.347	<0.0001	0.323	0.79 ± 0.30	5.0 ± 10.2
log Eddington ratio	$\log L_{\rm core}$	7	Seyfert	K	0.591	0.0149	0.582	0.98 ± 0.36	37.6 ± 13.4
$0.83 \log L_{\rm [O\,iii]} + 0.82\, M_{\rm BH}$	$\log L_{\rm core}$	8	Seyferts	K	1.072	0.0007	–	0.84 ± 0.21	3.3 ± 10.2
$0.83 \log L_{\rm [O\,iii]} + 0.82\, M_{\rm BH}$	$\log L_{\rm core}$	8	RL AGN + 3C/FR I	P	0.886	3.8×10^{-9}	–	1.20 ± 0.15	-9.1 ± 6.1
$0.83 \log L_{\rm [O\,iii]} + 0.82\, M_{\rm BH}$	$\log L_{\rm core}$	8	RQ LINERs	S	0.543	<0.0001	–	0.83 ± 0.19	4.0 ± 9.5
$0.83 \log L_{\rm [O\,iii]} + 0.82\, M_{\rm BH}$	$\log L_{\rm core}$	8	Non-jetted HII	S	0.426	<0.0001	–	0.60 ± 0.25	13.0 ± 12.9

Note. Column description: (1)–(2) the two variables of the considered relation; (3) figure; (4) the sub-sample of galaxies for the tested correlation. 'Active galaxies' include AGN (LINER and Seyferts) and jetted (ALG and H II) galaxies; (5)–(7) the statistical analysis used for the given sub-sample to calculate the associated linear regression coefficient $\rho_{\rm XY}$ and the probability that there is no correlation $P_{\rho_{XY}}$: S for the censored generalized Spearman's correlation coefficient (for >30 objects), K for the censored generalized Kendall's τ correlation coefficient (for <30 objects), and P for the Pearson correlation coefficient for fully a detected data set; (8) censored partial rank correlation coefficient between X and Y adjusting for the target distance D; and (9)–(10) the slope and the intercept of the best fits with their 1-σ errors.

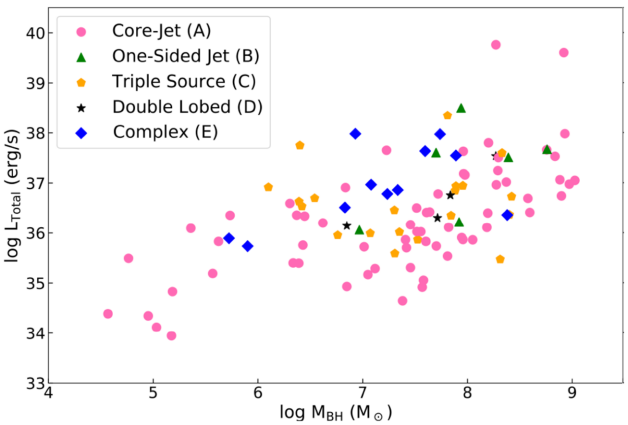

Figure 5. The total 1.5-GHz luminosity ($L_{\rm Total}$ in erg s^{-1}) as a function of the BH masses (M$_\odot$) for the LeMMINGs sample, divided per radio morphological classes A, B, C, D, and E (symbol and colour coded according to the legend).

the accretion, instead of the X-ray luminosity and found an analogous correlation for active BHs. The advantage of using the [O III] line instead of the X-ray data is the accessibility from the ground with reasonable resolution. Full coverage of the optical and radio data for the entire LeMMINGs sample allows a complete analysis of the fundamental plane (FP). New X-ray *Chandra* observations and the X-ray-based FP of the LeMMINGs sample will be addressed in forthcoming papers (Williams et al. 2021).

Fig. 8 depicts the optical FPBHA of the LeMMINGs galaxies by using the same parametrization expressed by Saikia et al. (2015). Note that these authors used 15-GHz *VLA* observations at a resolution of $\sim$0.″13, comparable with that of our *e*-MERLIN data. Yet, their observations are possibly less contaminated by SF and more sensitive to the nuclear optically thick radio emission than our 1.5-GHz observations because of the higher radio frequency.

In Paper I, despite a limited number of sources, we noted that the active galaxies appear to broadly follow a common correlation in the optical FP, stretching their luminosities up to FR I RGs. Nevertheless, Paper I also noted that the three classes are slightly stratified within the FP scatter across the radio luminosities, possibly reminiscent of the different accretion states for each optical class. Here, thanks to the sample completeness, we are able to recognize that different optical classes move separately along the plane. LINERs still appear to follow the FR Is at lower luminosities. The RL (FR I, Parma et al. 1986) jetted H II, NGC 3665, lies on the RL AGN relation and the rest of the jetted H II galaxies agree with the FPBHA of RQ LINERs. Seyferts, on the other hand, seem to cover a different sequence in the plane because of their lower radio-core luminosities. Non-jetted star-forming galaxies stand out from the rest of the sample because of their smaller BH masses and lower [O III] and radio luminosities. Therefore, similar to the approach taken in Paper I, we prefer to fit the FPBHA for the different classes by using the parametrization introduced by Saikia et al. (2015) (in units of erg s^{-1} for luminosities and M$_\odot$ for BH masses)[7]:

$$\log L_{\rm core} = (0.83\ \log L_{\rm [O\,iii]} + 0.82\ \log M_{\rm BH})\, m + q,$$

where Saikia et al. found $m = 1.0$ and $q = -3.08$ for their sample. Table 2 collects all the statistical results obtained from fitting the FP for different classes. Seyferts exhibit a tight linear correlation even evident to the naked eye, with a slope of $m = 0.84 \pm 0.21$. The generalized Kendall's τ coefficient of the Seyfert FP is 1.072, which indicates that two axis quantities do not correlate with a probability of 0.0007. The whole LINER population shows a large scatter in the FP. A better understanding of this population is possible by separating RL and RQ LINERs, which follow different tracks in Fig. 8: RL

[7]We refrain from providing a new optical FPBHA parametrization independent of that of Saikia et al. because of the presence of a large fraction of upper limits in radio and [O III] data and the fact that [O III] luminosity is not an absolute estimator of the AGN activity. We will dedicate an accurate analysis on the X-ray-based FPBHA by using the state-of-the-art censored-data statistics (Williams et al. 2021).

Downloaded from https://academic.oup.com/mnras/article/508/2/2019/6385009 by guest on 03 September 2022

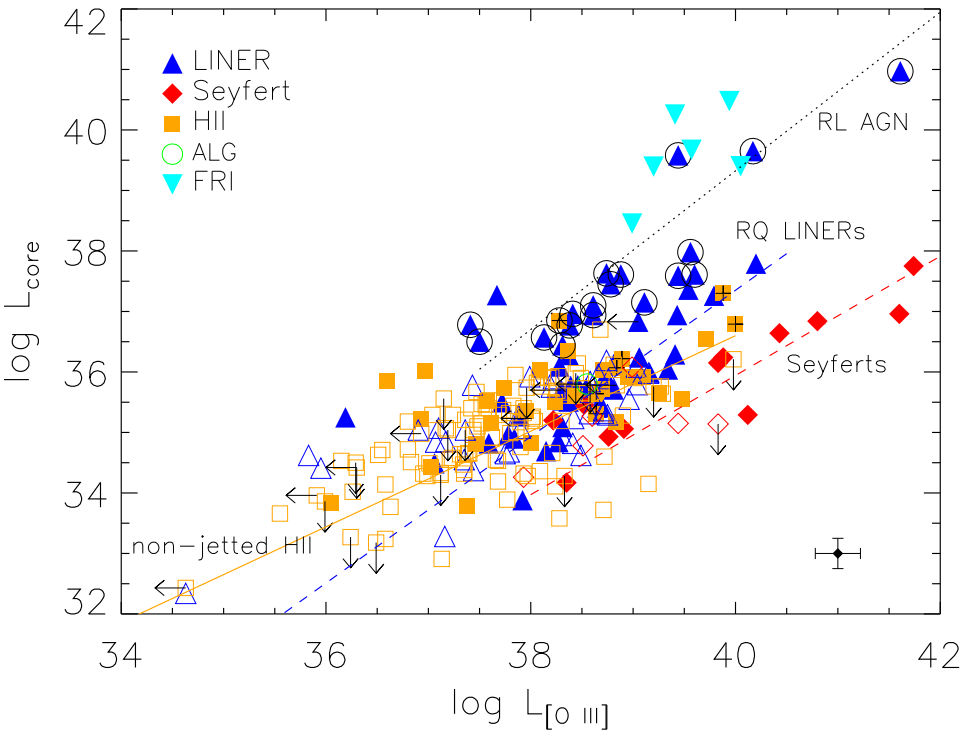

Figure 6. [O III] line luminosity ($L_{[\mathrm{O\,III}]}$ in erg s^{-1}) versus 1.5-GHz core luminosities (L_{core} in erg s^{-1}) for the LeMMINGs sample. The different optical classes are coded (symbol and colour) according to the legend of Fig. 2. The jetted H II galaxies show an additional plus sign. The filled symbols refer to the detected radio sources, while the empty symbols refer to non-detected radio sources (3σ upper limits). The unidentified sources (detected but the radio core has not been identified) are the empty symbols with radio 3σ upper limits. The dotted line represents the linear correlation by fitting only the RL AGN (black circles) together with the 3C/FR Is, the blue dashed line represents the fit by including RQ LINERs, the red dashed line for Seyferts, and the yellow triple-dot–dashed line for non-jetted H II galaxies (see Table 2 for best-fitting parameters). The black bars in the bottom right corner indicate the typical errors for the data points.

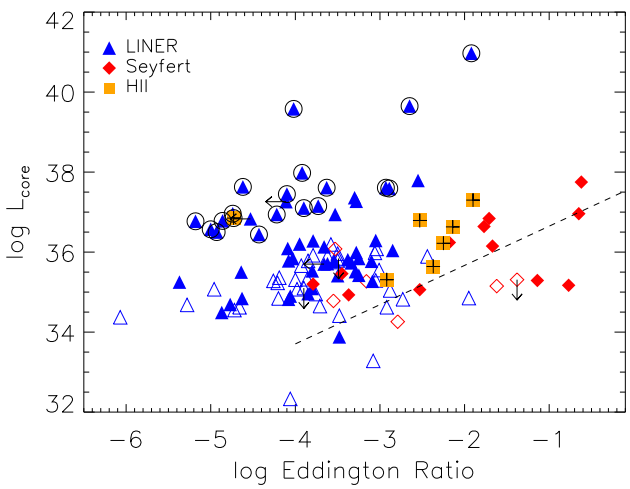

Figure 7. Eddington ratio (whose bolometric luminosity is estimated from $L_{[\mathrm{O\,III}]}$, see Section 2.1) versus 1.5-GHz core luminosity (erg s^{-1}) only for active galaxies (LINER, Seyferts, and jetted H II galaxies, and no ALGs for the lack of their optical counterparts). Symbols and colours, described in the legend, are coded analogously to Fig. 2. The dashed line represents the best fit for Seyferts (by using censored-data statistics, see Table 2).

LINERs extend the FR Is to lower regimes, whereas RQ in general tend towards the locus of Seyferts. We search for linear correlations separately for the two LINER classes. For RL AGN (RL LINERs + FR Is), the fit clearly appears steeper than the Seyfert plane, with a slope of $m = 1.20 \pm 0.15$ (Pearson's P value $= 3.8 \times 10^{-9}$). For the RQ LINERs, the plane is statistically consistent with the one defined by Seyfert galaxies but it extends to lower luminosities with a larger scatter, bridging the gap between RL LINERs and Seyferts: $m = 0.83 \pm 0.19$ with a (Spearman's) P value <0.0001. The non-jetted H II galaxies break the generic FP of the active galaxies with a flatter slope ($m = 0.60 \pm 0.25$, Spearman's P value <0.0001) extending to the lowest luminosities and BH masses of the sample.

Although L_{core} has been found to correlate with both M_{BH} and $L_{[\mathrm{O\,III}]}$ for the LeMMINGs sample (Sections 3.1 and 3.2), a mutual dependence could stretch the optical FPs we observe. The scatters of the FPs of the optical classes (FWHM <0.8 dex) are typically smaller than the scatters of the relations defined for each class in the radio-M_{BH} and the radio-[O III] planes (FWHM <1 dex). This suggests that the observed FPs are not stretched by any particular dependence on one of the three quantities (L_{core}, M_{BH}, and $L_{[\mathrm{O\,III}]}$), which establish the plane, as it has been also confirmed by other studies (e.g. Saikia, Körding & Dibi 2018a). Nevertheless, the large number of upper limits in the radio and line measurements may undermine the reliability of the fitted FPs. To test the accuracy of the established FPs, in the cases of non-detected Seyfert and LINER galaxies in the radio band, if we assign a core luminosity extrapolated by the M_{BH}–L_{core} relation found for active galaxies, the corresponding data points would lie on the plane of their corresponding class. Analogously, non-detected ALGs (in [O III] but detected in radio) would sit between RL and RQ LINERs. Conversely, non-jetted H II galaxies would follow the plane of the RQ LINERs if they had the core luminosities assigned by the M_{BH}–L_{core} relation valid for AGN at their BH masses. This result reinforces the discrepancies of the observed FPs and their physical meanings for the different optical

Downloaded from https://academic.oup.com/mnras/article/508/2/2019/6385009 by guest on 03 September 2022

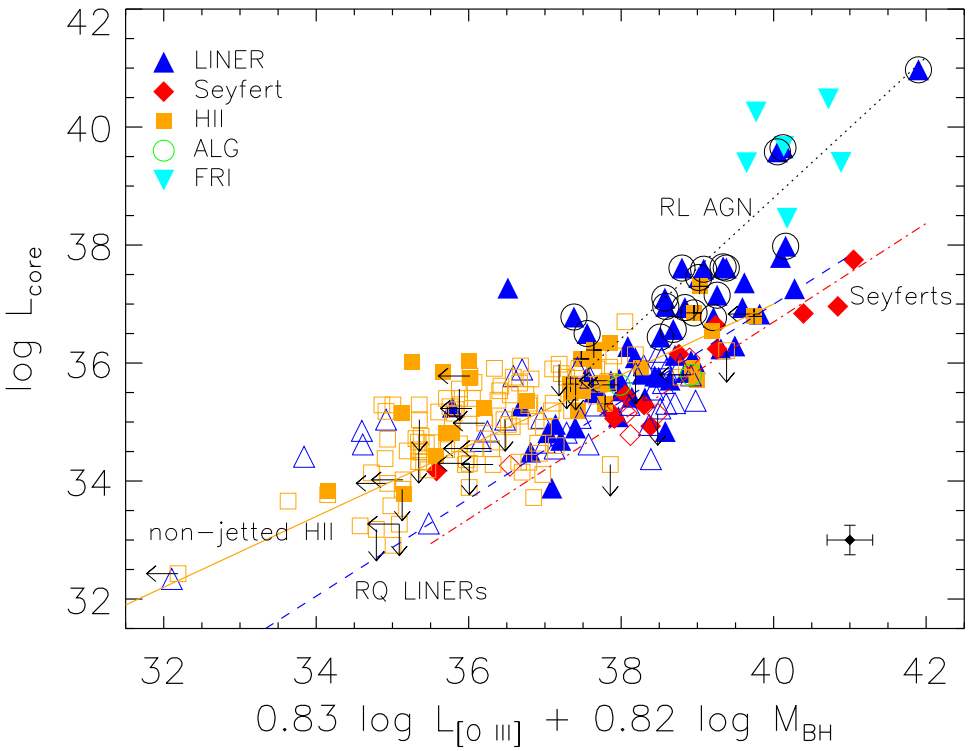

Figure 8. The fundamental plane of BH activity (FPBHA) in the optical band for the LeMMINGs sample with *e*-MERLIN data, i.e. $L_{\rm core}$ versus 0.83 × log $L_{\rm [O\,III]}$ + 0.82× log $M_{\rm BH}$ (1.5-GHz core and [O III] luminosities in erg s^{-1} and BH masses in M$_\odot$) parametrized as expressed by Saikia et al. (2015). Colour and symbols are explained in the legend. The filled symbols refer to the detected radio sources, while the empty symbols refer to non-detected radio sources (3σ upper limits). The unidentified sources are the empty symbols with radio 3σ upper limits. The dotted line represents the best fit for RL AGN (large black circles) and 3C/FR Is, the blue dashed line represents the fit for RQ LINERs, the red dot–dashed line for Seyferts, and the yellow triple-dot–dashed line for non-jetted H II galaxies (see Table 2 for best-fitting parameters using censored-data statistics). The black bars in the bottom right corner indicate the typical errors for the data points.

classes. In summary, star-forming and active galaxies follow different FPs, as also evident in the radio-[O III] plane (Fig. 6), which are likely a consequence of different origins of their radio emission in relation to their main source of energy (stellar or BH accretion).

4 DISCUSSION

The LeMMINGs survey has unveiled radio cores at the centre in around half of our sample of local Palomar galaxies. Here, we investigate the origin of the nuclear 1.5-GHz emission and discuss the optical–radio association in the context of physical models of disc–jet coupling[8] and SF for each optical class (see Table 3 for a simple summarizing sketch; see also Panessa et al. 2019).

4.1 LINERs

LINERs are among the most frequently detected and most luminous sources in the LeMMINGs sample. They are mostly detected in ETGs and feature bright radio cores and jets.

Near-infrared, optical, and X-ray nuclear emission in LINERs has generally been interpreted as related to an active SMBH (Terashima et al. 2002; Balmaverde, Capetti & Grandi 2006; Flohic et al. 2006; González-Martín et al. 2006; Kharb et al. 2012), although reservations have been raised in the past (e.g. stellar-dominated optical nuclei, Capetti 2011). In contrast, several pieces of evidence convincingly argue in favour of an AGN origin of the radio emission in LINERs. First, their high brightness temperatures measured with *e*-MERLIN and VLBI ($T_{\rm B} > 10^7$ K, Papers I and II, Falcke et al. 2000) suggest synchrotron emission from (mildly to highly) relativistic jets. Secondly, core luminosities for LINERs correlate with their BH masses up to the classical RL regime with $M_{\rm BH} \sim 10^9 M_\odot$, suggesting that the mass of the SMBH plays a major role in the production of radio emission. Thirdly, LINERs are often associated with either symmetric or asymmetric pc/kpc-scale jets with luminosities of $\sim 10^{36}$ erg s^{-1}, similar to low-power RGs (Fanti et al. 1987). Such morphologies and powers cannot easily be explained by SF, as the latter resides in the sub-mJy regime below 10^{34} erg s^{-1} (Bonzini et al. 2013; Mascoop

Table 3. Simplistic sketch of the origin of radio emission in relation to the accretion modes in local galaxies.

Class	Radio	$\dot{m}$	Disc
RL LINER	Relativistic jets	$\lesssim 10^{-3}$	RIAF
RQ LINER	Sub-relativistic jets	$\lesssim 10^{-3}$	Truncated thick disc
(RQ) Seyfert	Sub-relativistic jets	$\lesssim 10^{-2}$	JED/truncated slim disc
	Disc/corona wind	$\gtrsim 10^{-2}$	SAD
ALG	(Sub-)relativistic jets	$\lesssim 10^{-3}$	Recurrent/starving RIAF
Jetted H II	Sub-relativistic jets and SF	$\lesssim 10^{-3}$	RIAF?
Non-jetted H II	SF		

Note. Column description: (1) optical class; (2) radio properties: sub-/relativistic jets, disc, or magnetically active corona wind, and SF; (3) Eddington-scaled accretion rate $\dot{m}$; and (4) disc mode (see Sections 4.1–4.4 for details).

[8]Disc–jet coupling refers to the connection between the inflowing accretion mode and the outflowing mode in the form of, e.g. jets, winds, or slow outflows (Panessa et al. 2019).

Downloaded from https://academic.oup.com/mnras/article/508/2/2019/6385009 by guest on 03 September 2022

et al. 2021). Fourthly, the jets tend to be core-brightened, similar to small FR Is (Capetti, Massaro & Baldi 2017), suggesting that the jets are probably collimated and launched relativistically on parsec scales but rapidly slow down along the jet propagation axis on kpc scales. These characteristics are similar to what is seen and modelled in nearby low-luminosity RGs (Morganti et al. 1987; Giovannini et al. 2005; Massaglia et al. 2016; Rossi et al. 2020).

The analysis of LINERs in this work has led to rather different results compared to what we found in Paper I, probably due to the inhomogeneous population of LINERs in the latter. Here, we identify two sub-classes, RL and RQ. A group of 18 RL LINERs have the lowest Eddington ratios ($\lesssim 10^{-4}$) and are the brightest sources of the sample. They typically reveal core–jet and twin jet morphologies, reside in ETGs, and extend the relations of 3C/FR Is to low radio and [O III] luminosities. The complementary RQ group of LINERs have slightly higher accretion rates than the RLs (Eddington ratios mostly $\sim 10^{-4}$–10^{-3}) and form an intermediate optical–radio relation between RL AGN and Seyferts.

Similarities in the correlations of RL LINERs and FR Is support the idea that they likely share the same central engine, capable of launching relativistic jets. The correlation between radio and optical (continuum) emission found for FR Is is best explained as the result of a single emission process in the two bands (i.e. non-thermal synchrotron emission from the base of the relativistic jet, Chiaberge, Capetti & Celotti 1999). Analogously, an [O III]-radio correlation found for FR Is and low-luminosity RL LINERs (Balmaverde & Capetti 2006) suggests a similar ionizing central source. Therefore, this interpretation is plausibly also valid for the RL LINERs in our sample, indicating that they represent the scaled-down version of FR Is with lower luminosities and accretion rates, as also reported in previous studies (Falcke et al. 2004; Allen et al. 2006; Balmaverde, Baldi & Capetti 2008). Multiple theoretical and analytical studies of FR Is (e.g. Meier 2001; Begelman 2012; McKinney et al. 2012) suggest that they are powered by an RIAF disc, usually as an advection-dominated accretion flow (ADAF, see reviews by Narayan & Yi 1994; Narayan & McClintock 2008), which can efficiently produce jets. As LINERs are usually radio-louder than the other optical classes and similar to low-power RGs (Capetti & Balmaverde 2006; Kharb et al. 2012), a model of an ADAF disc with a low-power jet (jet-dominated accretion flows, JDAF, Falcke et al. 2004) has been used as well to describe the disc–jet coupling of LINER-like AGN.

Conversely, the RQ LINERs appear to deviate from the RL AGN correlations, pointing to a different interpretation for their central engine. A possible truncated disc with an optically thick disc at larger radii (Chen, Halpern & Filippenko 1989; Maoz 2007; Narayan & McClintock 2008; Nemmen et al. 2014) could represent an intermediate regime between the low-$\dot{m}$ JDAF model for RL LINERs and high-$\dot{m}$ SAD models for luminous Seyferts. The accretion flow may begin as a thin SAD but, at a certain transition radius, gradually switches from a cold to a hot ADAF mode, resulting in composite characteristics with weaker sub-relativistic jets and slightly higher accretion rates. This result is broadly consistent with what has been found for a general dual population of RL and RQ LINERs in the local Universe (e.g. Chiaberge, Capetti & Macchetto 2005; Balmaverde & Capetti 2006).

4.2 Seyferts

Seyfert galaxies show the highest radio detection fraction in the LeMMINGs sample. Two-thirds of the detected Seyferts are found in spiral galaxies and one-third in ETGs. The Seyferts with the highest Eddington ratios and BH masses are the most luminous at 1.5 GHz, featuring edge-brightened radio morphologies.

Seyfert nuclei lie in a different region of the optical–radio plane with respect to RL LINERs and FR Is: for a similar radio luminosity, they show a significant optical excess (2–3 dex). On the one hand, their optical line excess is qualitatively similar to that observed in luminous type-I QSO, where their high-energy output is interpreted as a result of thermal emission from a radiatively efficient accretion disc (SAD, Cappi et al. 2006; Panessa et al. 2006; Singh, Shastri & Risaliti 2011). On the other hand, a large variety of radio characteristics observed in local Seyferts (e.g. morphologies, radio SED in relation to accretion properties, Laor et al. 2019) prevents a complete comprehension of the origin of their radio emission (Panessa et al. 2019; Silpa et al. 2020), although a non-thermal synchrotron origin for compact cores in Seyferts has been clearly established (Kukula et al. 1999; Mundell et al. 2000; Nagar et al. 2000; Ho & Ulvestad 2001).

As a first approximation, the radio *and* optical properties observed in our sample of Seyferts are consistent with the general properties of SADs: higher accretion rates ($>10^{-3}$ Eddington rate) and lower efficiency at launching and collimating jets than ADAF-dominated LINERs. In fact, diffuse lobe-like radio structures are observed more frequently in Seyferts than in LINERs in LeMMINGs and in other samples of local Seyferts (e.g. Kukula et al. 1993, 1995; Morganti et al. 1999; Gallimore et al. 2006; Kharb et al. 2006). These lobes[9] have been interpreted as sub-relativistic outflows at the core, which inflate bubbles and produce bow shocks in the ISM (Middelberg et al. 2004; Yuan & Narayan 2014).

To complete the puzzle, Seyferts are clearly radio-quieter than RQ LINERs, suggesting a different disc–jet coupling. Their strikingly distinct correlation between the radio core and disc luminosity and the lack of continuity between Seyferts and other AGN classes rule out the possibility that Seyfert jets are just the scaled-down versions of RG relativistic flows (Talbot, Bourne & Sijacki 2021). Our study also reveals a moderate increase of the radio luminosity and jetted structure fraction at higher Eddington ratios, which can be interpreted as increasing jet luminosity with higher $\dot{m}$ ($P_{\rm jet} = \eta_{\rm jet}\dot{m}c^2$ where $\eta_{\rm jet}$ is the jet production efficiency). This is different from the literature where there are reports of a tendency of an increased jet production ($\eta_{\rm jet}$) as the system goes fainter from QSOs to low-luminosity Seyferts (e.g. Trippe 2014; Wójtowicz et al. 2020), which is consistent with the anticorrelation between radio loudness and bolometric luminosity in AGN (e.g. Terashima & Wilson 2003; Panessa et al. 2007; Ho 2008) and in XRB (Fender, Homan & Belloni 2009). Such an effect could be caused by an incomplete separation between RQ and RL Seyferts and a lack of angular resolution to resolve jets. Previous studies were based on more heterogeneous samples of radio-emitting Seyferts/QSOs than our sample, which consists of a complete sample of resolved jetted RQ Seyferts. In fact, recent studies (Rusinek et al. 2020; Chang et al. 2021) that separate RQ and RL AGN show a slight $\eta_{\rm jet}$ increment to small Eddington ratios for RQ Seyferts, an effect that is enhanced by including RL Seyferts. Therefore, considering a differential dependence on $\dot{m}$ for each radio-emitting physical mechanism competing in the *total* radio production $\eta_{\rm radio}$ ($= \eta_{\rm jet} + \eta_{\rm disc\text{-}wind} + \eta_{\rm corona\text{-}wind}$) could

[9]We cannot fully rule out SF-driven super-winds as the cause of the observed lobes in Seyferts (Pedlar, Unger & Dyson 1985; Heckman, Lehnert & Armus 1993). However, such a scenario is unlikely because these structures are primarily observed in star-forming galaxies at low radio luminosities ($<10^{34}$ erg s^{-1}), where other than radio bubbles, extended SF in the galactic disc is observed.

Downloaded from https://academic.oup.com/mnras/article/508/2/2019/6385009 by guest on 03 September 2022

solve the tension (Laor et al. 2019). At low $\dot{m}$, a (core-brightened) sub-relativistic jet ($\eta_{\rm jet} > \eta_{\rm disc-wind} + \eta_{\rm corona-wind}$) might dominate over a (edge-brightened) radio-emitting disc/corona wind, which, in turn, becomes important at high $\dot{m}$ ($\eta_{\rm disc-wind}$ or $\eta_{\rm corona-wind} > \eta_{\rm jet}$) (see Section 4.5 for discussion and comparison with XRBs). Such scenario would account for both the heterogeneous radio properties of Seyferts and the general tendency of low-luminosity Seyferts to expel more compact jets than QSOs over a large range of Eddington ratios, covering the gap between two extreme classes: almost radio-silent high-$\dot{m}$ QSOs and jetted low-$\dot{m}$ LINERs. In addition, the role of the BH parameters (e.g. mass, spin) is to sustain and reinforce the jet/wind launch (Yang et al. 2021).

To accommodate the disc and radio similarities, respectively, with QSOs and LINERs, several scenarios have been proposed within the large breadth of SAD models. At small Eddington ratios, a solution could be the model of Jet Emitting Discs (JED, Ferreira et al. 2010), which are much less dense than an optically thick disc and arise at larger magnetization, where magneto-centrifugally driven jets are launched (Ferreira 1997). Another scenario is the presence of a truncated slim disc whose inner radius, where the jet is anchored, shrinks by dragging higher poloidal magnetic flux strength closer to a spinning SMBH. This condition favours the launch of strong radio outflows (Tchekhovskoy, Narayan & McKinney 2011) and leads to an increase of the jet Lorentz factor $\Gamma_{\rm jet}$, similar to what is seen in the hard-state XRBs (e.g. Fender, Belloni & Gallo 2004). At higher Eddington ratios, a quasar-driven uncollimated wind is favoured, able to shock the ISM, and accelerate relativistic electrons producing synchrotron radio emission (Faucher-Giguère & Quataert 2012; Zakamska & Greene 2014). An alternative scenario is an outflow of coronal plasma above the accretion disc, which slightly collimates within a narrow nozzle near the SMBH and then fans out to form a diffuse radio morphology (Donea & Biermann 2002; Markoff, Nowak & Wilms 2005; King et al. 2011; Raginski & Laor 2016).

4.3 Absorption line galaxies

The ALGs lack evidence of BH-accretion activity in the optical band but may still conceal a weak AGN at their centres, since they show bright radio cores and jets.

Apart from a few irregular/dwarf ALGs that are probably powered by stellar processes (Paudel & Yoon 2020), when detected in radio, ALGs appear indistinguishable from LINERs: massive ETGs hosting SMBHs with masses $\sim 10^8$ M$_\odot$ and core-brightened radio morphologies. In addition, the radio-detected ALGs are potential RL AGN, since their optical counterparts are not detected. This scenario is supported by a multiband study of local lineless RL AGN whose nuclei and hosts are similar to those of LINER-like RGs (Best et al. 2005b; Baldi & Capetti 2010) although at slightly higher luminosities than those of LeMMINGs sample (10^{39}–10^{41} erg s^{-1}). The radio detection of ALGs in this survey, and in previous studies, argues for the presence of an active SMBH in at least a quarter of ALGs. In this scenario, the optically weak characteristics of ALGs could also be reconciled with the picture of low-$\dot{m}$ RGs, where nuclear conditions (i.e. low ionizing source, poor gas availability) do not favour optical emission from a compact NLR. This picture has been observed in particularly faint FR Is (Buttiglione et al. 2009) and relic RGs (Capetti et al. 2013).

Even under favourable conditions, local SMBHs are known to exhibit levels of activity much lower than those expected from gas supplying rates on to the galactic nuclei, and only a small fraction of silent SMBHs can turn into AGN. Dynamic stability of gas reservoirs and particular conditions of magnetic field loops, which trap stars and gas in orbits, could lead to a fuel-starved SMBH (Inayoshi, Ichikawa & Ho 2020), thus resulting in ALGs. The problem of dormant massive BHs has much been discussed in the last decades (e.g Fabian & Canizares 1988; Kormendy & Ho 2001; Herpich et al. 2018) and the inactivity of ALGs falls in this investigation.

Another possible interpretation of the apparent absence of nuclear activity in ALGs is intermittent accretion (Czerny et al. 2009). For example, the currently quiescent Sgr A$*$ was recently found to have undergone a period of activity a few million years ago, which created a radio outflow as a consequence of an accretion event (Heywood et al. 2019). Around 30 per cent of fading AGN have been found to feature jets (Esparza-Arredondo et al. 2020). The large fraction of non-detected ALGs suggests that if they have intermittent periods of accretion activity, they are short-lived (10^4–10^5 yr, Reynolds & Begelman 1997). This is supported by estimates based on their radio jet lengths (Papers I and II). Any intermittent activity could be caused by occasional accretion events lasting a few Myr, where X-ray-emitting hot gas atmosphere, typical of ETGs (Forman, Jones & Tucker 1985), feeds the strangulated SMBH at a very low $\dot{m}$ and establishes a quasi-spherical accretion regime, which supports the jet launching (Ho 2002; Allen et al. 2006).

In summary, unfavourable nuclear conditions, SMBH dormancy, and nuclear recurrence can account for the optical and radio detections (or lack thereof) in ALGs. However, once the accretion is set, the activity phases visible in the two bands are not necessarily synchronized: the jet production can possibly lag the disc activity by a few 10^2–10^4 yr (depending on $M_{\rm BH}$ and jet length and power) as expected by disc–jet evolution models (e.g. Czerny et al. 2009).

4.4 H II galaxies

The H II galaxies are generally interpreted as SF-dominated nuclei, based on the emission line ratios in BPT diagrams, but this does not preclude them from having a weak AGN. H II galaxies show mostly compact single cores and extended complex structures.

The analysis of the full LeMMINGs sample confirms the results from Paper I: the presence of a dual population of H II galaxies, i.e. jetted and non-jetted, which are probably related to different origins of the core emission. In general, jetted H II galaxies are found to have larger $M_{\rm BH}$ ($\gtrsim 10^{6.5}$ M$_\odot$) than their non-jetted companions.

The vast majority of radio-detected H II galaxies are non-jetted. They are less [O III] luminous by a factor of $\sim$30 than active galaxies and typically have a large radio excess with respect to the [O III]–radio correlation found for LINERs at low $L_{\rm [O\,III]}$. All these characteristics are consistent with a scenario of a nuclear starburst on a scale of $<$1 kpc, producing stellar emission at 1.5 GHz. To corroborate this picture of a stellar origin, Paper I concluded that thermal/non-thermal and free–free radio emission predicted from supernova (SN) progenitors, SN explosions and SN remnants, and H II regions (Ulvestad, Wilson & Sramek 1981; Condon 1992) is sufficient to account for radio luminosities of non-jetted H II galaxies. In addition, a population of SNe expected from high SFR ($\sim$30–50 M$_\odot$ yr^{-1}) might be able to blow bubble-like super-winds (Weaver et al. 1977; Heckman et al. 2015), which would match the extended irregular morphologies (E class) observed in some sources.

In contrast, three aspects of the (seven) jetted H II sources point to the presence of an active SMBH, powering their radio emission: (i) larger BH masses than the non-jetted companions; (ii) core-brightened and elongated radio morphologies, and (iii) similar line-radio correlation and FPBHA to those found for RQ/RL LINERs. As an example, the well-known FR I (NGC 3665, Parma et al.

Downloaded from https://academic.oup.com/mnras/article/508/2/2019/6385009 by guest on 03 September 2022

1986) belongs to this sub-sample. We conclude that it is likely that this population of jetted H II galaxies does host weak AGN, whose output is too dim to significantly contribute to the optical emission, dominated by nuclear SF. The possible LLAGN signatures found in jetted H II galaxies are similar to those of sub-Eddington LINERs (likely powered by an RIAF), rather than the efficiently accreting Seyferts, and could represent the tip of the iceberg of a large population of weakly active sub-mJy star-forming galaxies at low powers (Padovani 2016; Muxlow et al. 2020). Another scenario to account for their radio-optical properties is the combination of both SF and an active BH in the event of a jet shocking a dense ISM and triggering *in situ* SF (Gaibler et al. 2012; Dugan et al. 2014). The SF–AGN coexistence underlines the symbiotic relationship between these two types of activity, particularly in LTGs (e.g. Santini et al. 2012).

4.5 Low-luminosity AGN and disc–jet coupling

Almost half (∼45 per cent) of the LeMMINGs galaxies are not radio silent but are characterized by low radio powers ($>10^{17.6}$ W Hz^{-1}). Our survey has revealed that local galaxies can show evidence of weak AGN-driven activity in the form of sub-galactic jets (B, C, and D classes) or optical line ratios (LINER or Seyfert) down to $L_{\rm core} \gtrsim 10^{18.7}$ W Hz^{-1}. By binning the sample by radio luminosity and BH mass, the fraction of radio detections reaches 100 per cent for galaxies with $L_{\rm core} \gtrsim 10^{19.8}$ W Hz^{-1} (twice than the survey sensitivity limit) and with $M_{\rm BH} \gtrsim 10^7$ M$_\odot$, regardless of optical type. This limit represents the lowest luminosity for which the most massive BHs hosted by local (Palomar) galaxies are 'always' switched on. This limit is lower than what has been obtained from previous radio surveys, $\sim 10^{20}$–10^{21} W Hz^{-1} for the most massive galaxies (Mauch & Sadler 2007; Cattaneo & Best 2009; Sabater et al. 2019).

Assuming that some (if not all) of the radio emission in LLAGN comes from jets, the jet fraction is expected to increase with decreasing Eddington ratios, and consequently, the radio loudness should increase with increasing BH mass (Ho 2008). However, the jet/radio properties of nearby galaxies have been shown to be more complicated than a simple bimodality (presence or lack of jet in relation of low- or high-$\dot{m}$ disc), suggesting specific modes of accretion and jet launching mechanisms for different optical AGN classes (Best & Heckman 2012; Hardcastle 2018). The high sensitivity and resolution of our survey cast light on the entanglement between radio/jet and optical/disc properties in LLAGN. Further help in disentangling this complexity comes from the comparison with the analogous disc–jet coupling observed in XRBs (Remillard & McClintock 2006; Fernández-Ontiveros & Muñoz-Darias 2021). Within the low/hard XRB state, there are indications that the transition radius between an inner ADAF and an outer thin disc decreases with increasing luminosity (Narayan 2005), and a short-lived strong radio outburst occurs where highly relativistic jets are launched (e.g. Fender et al. 2004). Conversely, clear jets are never seen in high-soft XRBs, while our survey and other studies demonstrate that their *putative* AGN-equivalent (low-luminosity) Seyferts can produce jets as much as LINERs do. While jetted AGN and low/hard XRBs clearly lie on the same FPBHA (Merloni et al. 2003; Falcke et al. 2004), Gültekin et al. (2019), by including radio-active high-/soft-state XRBs, cannot rule out that the latter and Seyferts are inconsistent with the FP made up of low-/hard-state XRBs and LINERs. Furthermore, Fischer et al. (2021) have recently shown that, Seyferts, once resolved with the VLBI on sub-parsec scales, can have corresponding $L_{\rm core}$ upper limits that are systematically below the predictions from the FPBHA. The tension with the analogies between stellar-mass BHs and active SMBHs probably rests on attempting to use the optical class to set the association. The Eddington-ratio argument could partially resolve this tension. For XRBs, sources are almost entirely in hard states below 2 per cent of $L_{\rm Edd}$ (Maccarone 2003; Vahdat Motlagh et al. 2019), while above that value both states are present. For AGN classes, LINER and Seyfert distributions usually roughly break up at 0.1 per cent of $L_{\rm Edd}$. Therefore, the global properties of LINERs (e.g. low Eddington ratios; weak or strong, persistent radio jets; hard X-ray spectra) make this class similar to hard-state XRBs. Conversely, Seyferts show more heterogeneous radio and disc properties and consist of a mixture of hard and soft states (Fernández-Ontiveros & Muñoz-Darias 2021). Low-$\dot{m}$ Seyferts (between 0.1 and 2 per cent of $L_{\rm Edd}$) could be more similar to hard XRBs and able to launch compact jets, while the high-$\dot{m}$ Seyferts are more similar to soft XRBs. However, as disclosed in Section 4.2, the current status of results on Seyferts based on radio observations reveals a higher level of complexity than this scenario. In fact, we would expect a larger fraction of jetted structures at low $\dot{m}$, similar to hard XRBs, which is opposite to what we observe in our sample, but in agreement if we consider a larger population that includes luminous Seyferts and QSOs. A possible explanation to this apparent contradiction is that different physical mechanisms of radio production coexist in Seyferts, which makes the comparison with XRBs even more challenging. At higher accretion rates ($\dot{m} \gtrsim 10^{-2}$), disc and corona wind are expected to play an important role in the radio emission (Laor et al. 2019) and could account for the observed tendency to display edge-brightened structures. At lower $\dot{m} \lesssim 10^{-2}$, a sub-relativistic compact jet, more similar to RQ LINERs, could dominate over the other radio-emitting physical processes (Table 3).

Although (simultaneous) high-frequency radio (e.g. mm-band) and X-ray observations would be ideal to isolate the pc-scale emission and its link to the disc (see Bell et al. 2011; Behar et al. 2020), in our 1.5-GHz survey, we observed a significant dependence of radio-optical properties (i.e. disc–jet coupling) with $M_{\rm BH}$. The small range of stellar BH masses of XRBs does not enable a straightforward comparison of radio models valid for XRBs with the results from the LeMMINGs survey. Instead, this is possible for AGN in general. In fact, AGN disc models predict different mass dependencies for the radio emission. The similar slopes found for RL and RQ AGN ($L_{\rm core} \propto M_{\rm BH}^{1.5-1.65}$) despite the large scatter can be interpreted as a single strong connection between the radio output and the BH mass, regardless of the type of the radio product (i.e. relativistic or sub-relativistic jets, winds, etc.). In the observed range of $L_{\rm core}$–$M_{\rm BH}$ slopes, a degeneracy of models exists: for jet-dominated sources (e.g. JDAF, Falcke et al. 2004), $L_{\rm radio} \propto \bar{a}^2 M_{\rm BH}$ (where $\bar{a}$ is the BH spin), ADAF models which predict radio emission $L_{\rm radio} \propto M_{\rm BH}^{8/5}\,\dot{m}^{6/5}$ (Yi & Boughn 1999), while relativistic jets can be described by the Blandford–Znajek (Blandford & Znajek 1977) process as $L_{\rm radio} \propto \bar{a}^2 M_{\rm BH}^2 B^2$ (where B is the magnetic field). Across the different AGN classes, a large range of BH spins, accretion rates, and magnetic field strengths could account for the significant but scattered relations we observe. The transition from RQ AGN (jetted H II galaxies, RQ LINERs, and Seyferts) to RL AGN (RL LINERs and FR Is) could be caused by an increment of BH or disc parameter values, which result in a boost of the radio emission (Blandford et al. 2019; Chen et al. 2021).

The radio emission production in XRBs is related to accretion rate and high-energy band luminosity (from optical to X-ray, produced by physical processes in disc and/or corona). Their jet contribution to

Downloaded from https://academic.oup.com/mnras/article/508/2/2019/6385009 by guest on 03 September 2022

the observed high-energy flux is largely debatable (e.g. Fender 2001; Markoff et al. 2003). Despite the problematic comparison between states of SMBHs and stellar BHs, radio and disc emission models of XRBs could still help to understand the physical processes involved in active SMBHs. For the jet-mode inefficient discs in XRBs, $L_{\rm radio} \propto L_{\rm X}^{0.5-0.7}$, whereas for disc-dominated sources, $L_{\rm radio} \propto L_{\rm X}^{1.4}$ (see Coriat et al. 2011). In our LeMMINGs sample, assuming that [O III] is a good indicator of the bolometric AGN power, which scales with the X-ray output, LINERs show a steeper radio–disc luminosity dependence ($L_{\rm core} \propto L_{\rm [O\,iii]}^{1.2-1.3}$ for RL and RQ LINERs) than Seyferts ($L_{\rm core} \propto L_{\rm [O\,iii]}$). This is opposite to the equivalent relationship observed in hard/soft XRBs. Furthermore, the absence of a clear dependence of the radio luminosity on Eddington ratios in LINERs casts new light on a possible disparity between jetted accreting compact objects, since hard-state XRBs show $L_{\rm radio} \propto \dot{m}^{1.4}$ (e.g. Körding et al. 2006), unless $L_{\rm [O\,iii]}$ scales as $\dot{m}$ for LINERs (Netzer 2009).

In the context of AGN models, for SAD-dominated sources the ratio $L_{\rm radio}/L_{\rm X} \propto \eta_{\rm jet}\,\bar{a}^2$ (Yi & Boughn 1999) is expected to be constant and limited to a narrow range of values, as we find for our Seyferts, if the $\bar{a}$ range is finite. Conversely, for LINERs, that are powered by RIAF discs, the relation between bolometric AGN and jet power is difficult to model because jet emission can dominate their entire SED (Körding, Jester & Fender 2008) and [O III]-line contamination from jet photoionizing shocks can overpredict the bolometric AGN power (Capetti, Verdoes Kleijn & Chiaberge 2005; Netzer 2009). However, in a simplistic scenario of a disc origin of the radio emission, ADAF discs would predict much shallower relations ($L_{\rm core} \propto L_{\rm X}^{\alpha}$ with α <0.6 depending on bremsstrahlung-dominated and multiple Compton scattering regimes, Yi & Boughn 1998) than the observed slopes for LINERs (1.2–1.3). Furthermore, the observed radio-[O III] relation found for LINERs is even steeper (despite the large scatter) than any previous relations between the kinetic jet power and the bolometric AGN luminosities found for LINER-like RL AGN (slopes <1, e.g. Capetti & Balmaverde 2006; Merloni & Heinz 2007; Baldi et al. 2019b). Therefore, assuming that RL LINERs are the scaled-down version of RGs and normalizing the $L_{\rm radio}/L_{\rm X}$ comparison with previous studies based on this assumption, the steeper slopes might be the consequence of a closer view of jet-launching mechanism even in RQ LINERs. The high sensitivity and sub-arcsec resolution (crucially intermediate between *VLA* and VLBI) provided by our survey allowed us to probe the parsec-scale region near the core where the jet is launched and reveal the relevant role of $\Gamma_{\rm jet}$ and BH spin/mass in the jet production. These parameters could eventually induce much steeper relations than those established with shallower radio observations.

Although the reliability of the [O III]–X-ray conversion could affect this comparison, the difference between AGN and XRBs is stark. In conclusion, the apparent disparity between AGN and XRB states suggests that LLAGN show different disc–jet couplings and more complicated mechanisms of radio production than the XRBs (without considering transition phases). However, a more detailed (radio/X-ray) study and comparison between LLAGN and XRBs is needed and is not the goal of this work.

Another variable that can increase the scatter of the observed radio–optical relations and complicate our comprehension of the disc–jet connection is the core variability. Radio flickering and transient events have been documented in the nuclei of some LLAGN, particularly Seyferts (e.g. Wrobel 2000; Mundell et al. 2009; Giannios & Metzger 2011; Baldi et al. 2015a; Mattila et al. 2018; Williams et al. 2019; Nyland et al. 2020).

4.6 Black hole – host connection

The LeMMINGs survey detected nuclear radio activity from high- down to low-mass galaxies ($L_{\rm bulge} \sim 10^9 - 10^{10.5} L_\odot$, Nagar, Falcke & Wilson 2005), which harbour SMBHs with masses $\gtrsim 10^{6.5}$ M$_\odot$. SF- and BH-driven radio emissions are the two main mechanisms responsible for the μJy-level radio-core emission (Padovani et al. 2015) with several pieces of evidence pointing to an increment of AGN contribution to radio emission as $M_{\rm BH}$ increases. In fact, the radio detection and the jet fraction increase with BH mass for $\gtrsim 10^{6.5}$ M$_\odot$ and the 'bulgeness' of the host (i.e. favouring ETGs, see Paper II).

One of the main results of our survey is the presence of a break of the empirical relations (radio, [O III], $M_{\rm BH}$, optical FPBHA) between the star-forming and active galaxies at $\sim 10^{6.5}$ M$_\odot$ (conservatively, between $\sim 10^6$ and $\sim 10^7$ M$_\odot$). A BH mass of $\sim 10^{6.5}$ M$_\odot$ seems to represent the turnover from an SF to an AGN regime as the BH mass increases. Such a break corresponds to the $M_{\rm BH}$, which roughly separates the BH mass function of local LTGs and ETGs (Davis et al. 2014; Greene, Strader & Ho 2020), i.e. pseudo-bulges and bulges (Yesuf et al. 2020) and SF- and AGN-dominated sources, respectively (see Kelly & Merloni 2012, Appendix A and Fig. A1). Both the fraction of galaxies that host a radio AGN and the radio-core powers correlate with $M_{\rm BH}$ with different relations at the two sides of this BH mass turnover. These relationships possibly agree with galaxy evolution models, which predict that high-mass galaxies evolve faster and host a radio-AGN that suppresses SF more effectively than low-mass galaxies (Fabian 2012), which instead form stars in the current Universe (e.g. Lapi et al. 2011; Behroozi et al. 2019). However, it is important to point out that such a break could also be the consequence of an intrinsic $M_{\rm BH}$-σ relation that flattens out at low BH masses (Mezcua 2017; Shankar et al. 2019).

Substantial progress in understanding the process of radio AGN phenomena in the nearby Universe has recently been made by combining optical and radio surveys to determine the statistical relationships between radio activity and galaxy/BH mass. It has been found that the fraction of galaxies that host RL AGN (with $L_{\rm radio} > 10^{21}$ W Hz^{-1}) is a strong function of stellar mass $\propto M_*^{2.5}$ and BH mass $\propto M_{\rm BH}^{1.6}$ (Best et al. 2005b; Mauch & Sadler 2007; Hardcastle et al. 2019; Sabater et al. 2019) with the most massive ETGs 'always' switched on at low radio powers ($\gtrsim 10^{21}$ W Hz^{-1}). In our statistically complete heterogeneous sample of local galaxies, mostly consisting of LTGs, we find a flatter dependence between the radio-AGN fraction $f_{\rm d}$ and BH mass for the active galaxies ($\propto M_{\rm BH}^{0.15}$), independent of the radio properties. The different slopes between our work and previous studies could be ascribed to three aspects: the higher angular resolution and higher sensitivity of our survey, crucial to identifying jets, the identification of genuine 'jetted' RQ AGN with respect to RL AGN, and a possible presence of a break in the radio luminosity function at $10^{19.5}$–10^{20} W Hz^{-1} (Nagar et al. 2005). This results in the inclusion of SMBHs with masses lower than those of standard RL AGN ($<10^8$ M$_\odot$), which can often emanate low-power jets on sub-kpc scale, despite their nominal radio-quietness definition, differently from the rarer powerful RGs. This selection eventually induces a much shallower dependence with BH mass. Janssen et al. (2012) also noted a shallower $f_{\rm d}$–$M_{\rm BH}$ relation than previous studies, scaling as $\propto M_*^{1.5}$, for Seyfert-like radio sources, which remains still steeper than what we found for RQ AGN. Moreover, in our survey, we do not find a clear separation (within the large scatter) between LINERs and Seyferts in the radio–$M_{\rm BH}$ plane. This likely indicates that accretion rate, which largely differs between the two classes, plays a more complicate role in the radio production, together with BH mass/spin (see Section 4.5).

Downloaded from https://academic.oup.com/mnras/article/508/2/2019/6385009 by guest on 03 September 2022

The observed correlation between $L_{\rm core}$ and BH mass or host type can also be an indirect consequence of a more fundamental relationship between radio luminosity and optical bulge luminosity (or mass) (Falcke et al. 2001; Ho 2002; Nagar et al. 2002): ETGs show larger radio luminosities than LTGs (Laor 2000; Decarli et al. 2007; Mauch & Sadler 2007; Gallo et al. 2008). The more massive elliptical galaxies or bulge-dominated systems are more efficient at producing radio emission as they have larger SMBHs and, hence, are more likely to be highly RL than spiral galaxies for $M_{\rm BH} > 10^8$ M$_\odot$ (Chiaberge & Marconi 2011). The high bulge-to-disc ratio is achieved in more evolved galaxies, where spheroids and pseudo-bulges dominate the central gravitational well. At their centres the extended jets expelled from accreting SMBHs can more easily plough through the more rarefied ISM than in discy (spiral) galaxies. Furthermore, according to the spin and gap paradigm (e.g. Moderski, Sikora & Lasota 1998; Garofalo, Evans & Sambruna 2010; Meier 2012), a higher BH spin and a larger gap region between the inner edge of the accretion disc, typically achieved in ETGs, can cause a larger magnetic flux accumulation on the SMBH and consequently a maximization of the BF jet mechanism. Such a condition is reached with retrograde accretion. Typically in LTG, a low-spinning SMBH and prograde disc have been suggested to account for their limited jet production compared to the different RL AGN classes found commonly in ETGs (RQ AGN against FR classes, see e.g. Tchekhovskoy & McKinney 2012; Garofalo, Kim & Christian 2014; Garofalo & Bishop 2020).

4.7 Star formation

Non-jetted H II galaxies clearly depart from the AGN classes in the optical–radio plane and FPBHA at low $L_{\rm core}$ and $M_{\rm BH} < 10^{6.5}$ M$_\odot$, showing a clear break likely caused by the increased SF contributions to the pc-scale radio emission. Such a sub-sample represents a much larger population of low-luminosity star-forming galaxies, which dominate the local Universe at $M_{\rm BH} < 10^{6.5}$ M$_\odot$ (Appendix A, Greene & Ho 2007; Greene et al. 2020), where stellar processes are generally the main source of energy.

Assuming that non-jetted H II galaxies are powered by SF, the relation between radio luminosities in such galaxies and $M_{\rm BH}$ can be deciphered as a link between thermal/non-thermal SF luminosity and BH mass, in the form $L_{\rm SF} \propto M_{\rm BH}^{0.61}$, which has the largest scatter of the observed linear regressions, due to the large uncertainties of $M_{\rm BH}$ estimates at low values and numerous radio non-detections. This unprecedented relation is likely the result of the observed link found between SF indicators such as radio, far-infrared, optical or line luminosities, and galaxy mass (e.g. Mauch & Sadler 2007; Gürkan et al. 2018). Moreover, the SF contribution in the radio band with respect to the AGN activity is expected to increase with galaxy mass (Aird, Coil & Georgakakis 2019). In fact, the observed correlation suggests that the radio production due to SF broadly increases with BH mass, as the latter quantity is approximately a constant proportion of the galaxy mass (from a third down to a fifth in the lowest $M_{\rm BH} \sim 10^5$ M$_\odot$, Häring & Rix 2004; Reines & Volonteri 2015; Martín-Navarro & Mezcua 2018), i.e. the stellar content: more stars likely produce more radio emission. This is consistent with the idea that SF, although mostly included in the disc (Bluck et al. 2020) and known to scale with galaxy mass (Speagle et al. 2014), would possibly also scale with $M_{\rm BH}$. More precisely, the nuclear starburst is plausibly set by the available gas mass present in the NSC ($M_{\rm NSC}$, Fernández-Ontiveros, Prieto & Acosta-Pulido 2009; Neumayer, Seth & Böker 2020), which scales with the galaxy dynamical mass ($M_{\rm NSC} \propto M_{\rm dyn}^{0.55}$, Scott & Graham 2013), which in turn respond to the SMBH gravitational well (Cen 2015; Pitchford et al. 2016). Such a sequence of links eventually enacts the radio-$M_{\rm BH}$ and radio-optical relations observed for star-forming galaxies, e.g setting the fraction of radio emission with respect to the photoionizing energy from young stellar populations and SN products.

Using the [O III] as an SF indicator (Suzuki et al. 2016), the observed optical luminosities of non-jetted H II galaxies can be interpreted by an SFR up to $10^{1.1\pm0.5}$ M$_\odot$ yr^{-1} in a nuclear starburst. The [O III]-radio correlation valid for non-jetted H II galaxies also represents an empirical method to predict the nuclear radio emission in star-forming galaxies based on the ubiquitous [O III] line data. The best fit approximately agrees with the [O III]–radio relation estimated from *Herschel*, *LOFAR*, and *VLA* data ($L_{1.4\,\rm GHz} = [0.83 \pm 0.10] \log L_{\rm [O\,III]} + [7.9 \pm 2.0]$, Best et al. 2005a; Gürkan et al. 2015, 2018), although our observations are at a higher resolution than any previous study on large samples of star-forming galaxies.

5 REVIEWING THE RADIO PROPERTIES OF LOCAL GALAXIES

5.1 The LeMMINGs view

The 1.5-GHz LeMMINGs survey has revealed pc-scale cores and jet-like structures in more than a third of local optically active and inactive Palomar galaxies (Papers I and II). Such nuclei are part of a large population of radio LLAGN and faint nuclear starbursts ($\gtrsim 10^{17.6}$ W Hz^{-1}). This result adds observational evidence that a large fraction of LLAGN (even RQ AGN) feature low-power galactic-scale jets (Webster et al. 2021), which may have a tremendous impact on their hosts by continuously injecting energy, a fundamental ingredient for galaxy feedback (Morganti 2017; Jarvis et al. 2019; Hardcastle & Croston 2020; Smith et al. 2020b; Jarvis et al. 2021; Venturi et al. 2021), as supported by the state-of-the-art jet simulations (Massaglia et al. 2016; Mukherjee et al. 2018, 2020).

In this work, we have investigated the nature of the pc-scale nuclear radio components of LINERs, Seyferts, ALG, and HII galaxies. The emission-line [O III] luminosity, available for the entire sample, gives the optical nuclear counterpart of the 1.5-GHz cores we detected. The optical–radio connection and the optical FPBHA (Saikia et al. 2015) probe the different physical processes involved at the centre of galaxies. In these diagnostic diagrams, we have found that optical classes follow distinct tracks: this is indicative of different physical processes responsible for the radio emission and broadly agrees with previous multiband studies of LLAGN and star-forming galaxies (e.g. Körding et al. 2006; Vitale et al. 2015; Tadhunter 2016; Mancuso et al. 2017; Smith et al. 2020a). None the less, we have set more robust constraints on these trends with respect to previous studies and Paper I, especially in the thus far poorly explored regime of low luminosities and BH masses, by leveraging the unprecedented completeness and depth of the LeMMINGs survey.

.

LINERs are divided into two classes: RQ and RL. The RL LINERs (∼19 per cent of LINERs) appear to represent the scaled-down version of FR Is at lower radio and [O III] luminosities and BH masses down to $\sim 10^{7.5}$ M$_\odot$. Our results indicate that the class of RL LINERs belongs to a large homogeneous population of RL LLAGN ($< 10^{42}$ erg s^{-1}), characterized by a broad and continuous distribution of parameters of relativistic jets (e.g. sizes, luminosities, $\Gamma_{\rm jet}$), powered by a sub-Eddington, RIAF-like disc, and hosted in ETGs (Heckman & Best 2014). This picture, in turn, suggests that a common jet-launching mechanism operates in all RL LINERs, which smoothly connects low-power (sub)kpc-scale jetted LINERs to more powerful compact RGs (named FR 0s, Baldi, Capetti & Giovannini

Downloaded from https://academic.oup.com/mnras/article/508/2/2019/6385009 by guest on 03 September 2022

2015b) and full-fledged FR Is and FR IIs (Kharb et al. 2014; Mingo et al. 2019; Grandi et al. 2021). Conversely, RQ LINERs consist of a more heterogeneous population of LLAGN, which can reside in either LTGs or ETGs. An intermediate disc between low-$\dot{m}$ ADAF and high-$\dot{m}$ SAD may be consistent with the observed characteristics of RQ LINERs, where radio emission is due to a low-power non-relativistic uncollimated jet (Gallimore et al. 2006).

Seyfert nuclei radiate at a larger fraction of Eddington luminosity than LINERs. The common picture is that Seyferts are powered by a radiatively efficient SAD with higher accretion rates (Eddington ratios $\gtrsim 10^{-3}$) than seen in LINERs. Nevertheless, Seyferts are not radio-silent at all and can show compact or edge-brightened jetted morphologies. In order to reconcile their radio and optical properties, different disc–jet models, intermediate between jetted LINERs and the 'radio-silent' near-Eddington QSOs (Balick & Heckman 1982; Liu et al. 2020), have been proposed. Low-$\dot{m}$ Seyferts are possibly the scaled-down version of the so-called red QSOs, which have intermediate radio loudness and have been found to have a higher incidence of compact and extended radio morphologies than blue QSOs (e.g. Klindt et al. 2019; Rosario et al. 2020), which instead are more similar to high-$\dot{m}$ Seyferts. We conclude that the change of disc–jet coupling from low-power Seyferts to powerful QSOs and the predominance of a specific radio-emitting physical process may depend on different factors (Garofalo & Bishop 2020): the jet efficiency with respect to the disc- or corona-wind radio production decreases with Eddington ratio and increases with BH mass, 'bulgeness' of the host (favouring ETGs), and SMBH/disc spin.

Apart from a few irregular galaxies, the vast majority of ALGs are hosted by massive ETGs with $M_{\rm BH} > 10^7$ M$_\odot$, which lack significant optical emission from the nucleus. They have been interpreted as part of a large population of evolved massive galaxies (Salucci et al. 1999), which occasionally or recurrently go through periods of LINER-like low-$\dot{m}$ activity, during which they launch pc-scale jets. However, during this low-activity phenomenon, the optical line nucleus remains quiescent due to the combination of a low ionizing radiation field produced by the disc (and jet) and the rarefaction of cold gas to photoionize (Capetti et al. 2005).

A dual population of H II galaxies has been found in our sample. On one hand, the majority of the H II galaxies are hosted in LTGs with $M_{\rm BH} \lesssim 10^{6.5}$ M$_\odot$ and their optical–radio properties reconcile with an SF origin. An SF rate of $\sim$10 M$_\odot$ yr^{-1} in the central region can account for their compact cores, with SN-driven winds (Heckman et al. 2015) or extended H II regions possibly causing their complex radio structures. On the other hand, $\sim$5 per cent of H II galaxies exhibit jet-like radio structures. These sources follow the diagnostic optical–radio sequence of AGN-classed sources with $M_{\rm BH} \gtrsim 10^{6.5}$ M$_\odot$. The coexistence of a LINER-like sub-Eddington accreting SMBH and a nuclear starburst, which are responsible for the radio/jet and the optical properties, respectively, is the simplest way to solve their puzzling nature (Padovani 2016).

5.2 Conclusions

The LeMMINGs survey characterizes radio activity (either from SF or AGN) from a complete sample of local galaxies by reaching a 100 per cent detection rate for galaxies with $M_{\rm BH} > 10^7$ M$_\odot$ down to luminosities $L_{\rm core} > 10^{19.8}$ W Hz^{-1}. This limit represents the lowest luminosity for which galaxies appear to host a radio-active SMBH in the local Universe. The fraction of radio-active galaxies scales as $\propto M_{\rm BH}^{0.15}$, a relation that is flatter than what has been found in previous radio surveys (e.g. Best et al. 2005b), probably because of higher angular resolution and the inclusion of RQ AGN.

One of the main results of our survey is the presence of a break at $M_{\rm BH} \sim 10^{6.5}$ M$_\odot$ moving from the SF to AGN regime with increasing BH mass. Such a $M_{\rm BH}$ value roughly separates the star-forming galaxy and (LL) AGN populations in the local Universe. At larger BH masses, mostly in ETGs, a link between SMBH activity and jet production is well established (e.g. Cen 2012; Heckman & Best 2014). In contrast, in less-massive (late-type) galaxies, SF makes a proportionally larger contribution to radio luminosity causing a flattening of the relations valid for AGN at lower $M_{\rm BH}$.

For galaxies with small BH masses, $\lesssim 10^{6.5}$ M$_\odot$, thermal/non-thermal emission from stellar processes in star-forming galaxies is the most plausible scenario of the origin of their radio emission. An unprecedented empirical relation between their nuclear radio emission and BH masses, $L_{\rm core} \propto M_{\rm BH}^{0.61}$, has been inferred in our sample (although with large scatter). This relation between the nuclear SF and the SMBH was found as a result of the *e*-MERLIN array, able to resolve out smooth, extended emission and reveal the radio emission at the nuclear scale, where the central starburst is more likely to respond to the influence of the central SMBH.

The steepening of the empirical correlations found for galaxies with BH masses $\gtrsim 10^{6.5}$ M$_\odot$ ($L_{\rm core} \propto M_{\rm BH}^{1.5-1.65}$ and radio-AGN fraction $\propto M_{\rm BH}^{0.15}$) with respect to those at lower BH masses (valid for star-forming galaxies) strongly invokes an active SMBH as the main driver of their radio emission. The link between radio activity, SMBH properties, and local conditions (e.g. host type, gas availability) appears more complicated than the standard BH–disc bimodality deduced from galaxy–SMBH models (Heckman & Best 2014) or direct analogies with XRBs states (Remillard & McClintock 2006; Fender et al. 2009): low-$\dot{m}$/jet versus high-$\dot{m}$/no-jet. As a first approximation, the Eddington-scaled accretion rates ($\dot{m}$) of the sample correspond to two extreme radio and host categories. The most massive and bulged galaxies, which are the radio loudest with the (optically) faintest nuclei (LINERs, ALGs, and jetted H II galaxies), are powered by sub-Eddington ($\dot{m} \lesssim 10^{-3}$) RIAF-like discs and launch the most core-brightened jets. In contrast, LTGs can host high-$\dot{m}$ ($\dot{m} \gtrsim 10^{-3}$) standard disc and occasionally support sub-relativistic edge-brightened jets. As a second-order approximation, a closer inspection of the data reveals that optical classifications do not simply map the accretion states and this can further complicate the comparison with XRBs. Therefore, to break the degeneracy between radio loudness, accretion modes, and host types, distinct disc–jet couplings (accretion/ejection states) that are observed among the various optical–radio classes (RL/RQ, LINER/Seyfert, SF/AGN-dominated) are required. The connection between disc and jet is probably determined by a combination of several factors (some not directly observable at present), including BH spin, magnetic field strength, accretion rotation, gas supply, small- and large-scale environment, and host location within the environment (e.g. distance from cluster centre). These parameters play a significant role in setting the generic disc configuration (e.g. accretion mode, rate, and radiative efficiency) and the radio production mechanism (e.g. jet, outflow, wind) for each optical/radio class. Variation of these factors could favour the increase of the jet production efficiency and/or jet bulk speed (Lagos, Padilla & Cora 2009). This picture would account for the continuous, rather than dichotomous, radio properties observed in LLAGN, which are characterized by a broad distribution of sizes and luminosities of their extended radio emission, from weak RQ LINER (even ALG) to RGs and from jetted low-power Seyferts to extremely RQ high-$\dot{m}$ QSOs (Brown et al. 2011; Garofalo et al. 2014; Kharb et al. 2014; Baldi et al. 2019a; Garofalo & Singh 2019). A time-dependent evolution among different radio/optical states would add a further level of complexity to this picture, probably in analogy

Downloaded from https://academic.oup.com/mnras/article/508/2/2019/6385009 by guest on 03 September 2022

to XRB intermediate states (Fernández-Ontiveros & Muñoz-Darias 2021). An exhaustive comparison between LLAGN and XRBs will be addressed in a future work by using X-day data.

A complete census of the local SMBH population, offered by the forthcoming deep follow-up 5-GHz *e*-MERLIN observations along with complete *Chandra* X-ray and *HST* optical data, pushing to the rather unexplored regime of very low luminosities, $\sim 10^{16}$ W Hz^{-1} (comparable to Sgr A∗), will allow an unbiased view of the multiband SMBH activity of the local Universe and provide even more robust constraints on disc–jet coupling in LLAGN.

ACKNOWLEDGEMENTS

We thank the referee for his or her comments, which helped to improve the paper. This research was supported by a Newton Fund project, DARA (Development in Africa with Radio Astronomy), and awarded by the UK's Science and Technology Facilities Council (STFC) – grant reference ST/R001103/1. This research was supported by European Commission Horizon 2020 Research and Innovation Programme under grant agreement No. 730884 (JUMPING JIVE). FS acknowledges support from a Leverhulme Trust Research Fellowship. JHK acknowledges support from the European Union's Horizon 2020 research and innovation programme under Marie Skłodowska-Curie grant agreement no. 721463 to the SUNDIAL ITN network, from the State Research Agency (AEI) of the Spanish Ministry of Science and Innovation and the European Regional Development Fund (FEDER) under the grant with reference PID2019-105602GB-I00, and from IAC project P/300724, financed by the Ministry of Science and Innovation, through the State Budget and by the Canary Islands Department of Economy, Knowledge and Employment, through the Regional Budget of the Autonomous Community. IMV thanks the Generalitat Valenciana (funding from the GenT Project CIDEGENT/2018/021) and the MICINN (funding from the Research Project PID2019-108995GB-C22). AA and MAPT acknowledge support from the Spanish MCIU through grant PGC2018-098915-B-C21 and from the State Agency for Research of the Spanish MCIU through the 'Center of Excellence Severo Ochoa' award for the Instituto de Astrofísica de Andalucìa (SEV-2017-0709). BTD acknowledges financial support from grant 'Ayudas para la realización de proyectos de I + D para jóvenes doctores 2019' funded by Comunidad de Madrid and Universidad Complutense de Madrid under grant no. PR65/19-22417.

DATA AVAILABILITY

The data on which this paper is based are publicly available from the *e*-MERLIN archive. Calibrated image products are available upon reasonable request to the corresponding author. These, along with other LeMMINGs advanced survey products, will be publicly hosted on upcoming project web page, which is being developed (http://lemmingslegacy.pbworks.com).

REFERENCES

Aird J., Coil A. L., Georgakakis A., 2019, MNRAS, 484, 4360
Akritas M. G., Siebert J., 1996, MNRAS, 278, 919
Akritas M., 1989, Aligned Rank Tests for Regression With Censored Data. Penn State Dept. of Statistics Technical Report, p. 1989
Alexander D. M. et al., 2003, AJ, 126, 539
Allen M. G., Groves B. A., Dopita M. A., Sutherland R. S., Kewley L. J., 2008, ApJS, 178, 20
Allen S. W., Dunn R. J. H., Fabian A. C., Taylor G. B., Reynolds C. S., 2006, MNRAS, 372, 21
Aller M. C., Richstone D., 2002, AJ, 124, 3035
Baldi R. D. et al., 2018, MNRAS, 476, 3478
Baldi R. D. et al., 2021, MNRAS, 500, 4749
Baldi R. D., Capetti A., 2010, A&A, 519, A48
Baldi R. D., Behar E., Laor A., Horesh A., 2015a, MNRAS, 454, 4277
Baldi R. D., Capetti A., Giovannini G., 2015b, A&A, 576, A38
Baldi R. D., Rodríguez Zaurín J., Chiaberge M., Capetti A., Sparks W. B., McHardy I. M., 2019b, ApJ, 870, 53
Baldi R. D., Torresi E., Migliori G., Balmaverde B., 2019a, Galaxies, 7, 76
Baldwin J. A., Phillips M. M., Terlevich R., 1981, PASP, 93, 5
Balick B., Heckman T. M., 1982, ARA&A, 20, 431
Balmaverde B., Baldi R. D., Capetti A., 2008, A&A, 486, 119
Balmaverde B., Capetti A., 2006, A&A, 447, 97
Balmaverde B., Capetti A., Grandi P., 2006, A&A, 451, 35
Barausse E., Shankar F., Bernardi M., Dubois Y., Sheth R. K., 2017, MNRAS, 468, 4782
Begelman M. C., 2012, MNRAS, 420, 2912
Behar E. et al., 2020, MNRAS, 491, 3523
Behroozi P., Wechsler R. H., Hearin A. P., Conroy C., 2019, MNRAS, 488, 3143
Bell M. E. et al., 2011, MNRAS, 411, 402
Bennett A. S., 1962, MmRAS, 68, 163
Best P. N., Heckman T. M., 2012, MNRAS, 421, 1569
Best P. N., Kauffmann G., Heckman T. M., Brinchmann J., Charlot S., Ivezić Ž., White S. D. M., 2005b, MNRAS, 362, 25
Best P. N., Kauffmann G., Heckman T. M., Ivezić Ž., 2005a, MNRAS, 362, 9
Beswick R., Argo M. K., Evans R., McHardy I., Williams D. R. A., Westcott J., 2014, Proceedings of the 12th European VLBI Network Symposium and Users Meeting (EVN 2014). Cagliari, Italy, p. 10
Binette L., Magris C. G., Stasińska G., Bruzual A. G., 1994, A&A, 292, 13
Bisogni S., Marconi A., Risaliti G., 2017, MNRAS, 464, 385
Blandford R. D., Znajek R. L., 1977, MNRAS, 179, 433
Blandford R., Meier D., Readhead A., 2019, ARA&A, 57, 467
Bluck A. F. L. et al., 2020, MNRAS, 499, 230
Bonchi A., La Franca F., Melini G., Bongiorno A., Fiore F., 2013, MNRAS, 429, 1970
Bonzini M., Padovani P., Mainieri V., Kellermann K. I., Miller N., Rosati P., Tozzi P., Vattakunnel S., 2013, MNRAS, 436, 3759
Brown M. J. I., Jannuzi B. T., Floyd D. J. E., Mould J. R., 2011, ApJ, 731, L41
Bundy K. et al., 2015, ApJ, 798, 7
Buttiglione S., Capetti A., Celotti A., Axon D. J., Chiaberge M., Macchetto F. D., Sparks W. B., 2009, A&A, 495, 1033
Buttiglione S., Capetti A., Celotti A., Axon D. J., Chiaberge M., Macchetto F. D., Sparks W. B., 2010, A&A, 509, A6
Cao X., 2007, ApJ, 659, 950
Capetti A., 2011, A&A, 535, A28
Capetti A., Baldi R. D., 2011, A&A, 529, A126
Capetti A., Balmaverde B., 2006, A&A, 453, 27
Capetti A., Balmaverde B., 2007, A&A, 469, 75
Capetti A., Massaro F., Baldi R. D., 2017, A&A, 598, A49
Capetti A., Robinson A., Baldi R. D., Buttiglione S., Axon D. J., Celotti A., Chiaberge M., 2013, A&A, 551, A55
Capetti A., Verdoes Kleijn G. A., Chiaberge M., 2005, A&A, 439, 935
Cappi M. et al., 2006, A&A, 446, 459
Cattaneo A., Best P. N., 2009, MNRAS, 395, 518
Cen R., 2012, ApJ, 755, 28
Cen R., 2015, ApJ, 805, L9
Chang N., Xie F. G., Liu X., Ho L. C., Dong A. J., Han Z. H., Wang X., 2021, MNRAS, 503, 1987
Chen K., Halpern J. P., Filippenko A. V., 1989, ApJ, 339, 742
Chen Y. et al., 2021, ApJ, 913, 93
Chiaberge M., Capetti A., Celotti A., 1999, A&A, 349, 77
Chiaberge M., Capetti A., Macchetto F. D., 2005, ApJ, 625, 716
Chiaberge M., Marconi A., 2011, MNRAS, 416, 917

Downloaded from https://academic.oup.com/mnras/article/508/2/2019/6385009 by guest on 03 September 2022

Cirasuolo M., Magliocchetti M., Celotti A., Danese L., 2003, MNRAS, 341, 993
Condon J. J., 1992, ARA&A, 30, 575
Coriat M. et al., 2011, MNRAS, 414, 677
Czerny B., Siemiginowska A., Janiuk A., Nikiel-Wroczyński B., Stawarz Ł., 2009, ApJ, 698, 840
Davis B. L. et al., 2014, ApJ, 789, 124
Davis S. W., Tchekhovskoy A., 2020, ARA&A, 58, 407
de Vaucouleurs G., de Vaucouleurs A., Corwin H. G., Jr, Buta R. J., Paturel G., Fouqué P., 1991, Third Reference Catalogue of Bright Galaxies. Volume I–III. Springer, New York
Decarli R., Gavazzi G., Arosio I., Cortese L., Boselli A., Bonfanti C., Colpi M., 2007, MNRAS, 381, 136
Dickson R., Tadhunter C., Shaw M., Clark N., Morganti R., 1995, MNRAS, 273, L29
Donea A.-C., Biermann P. L., 2002, PASA, 19, 125
Dopita M. A., Koratkar A. P., Allen M. G., Tsvetanov Z. I., Ford H. C., Bicknell G. V., Sutherland R. S., 1997, ApJ, 490, 202
Drappeau S. et al., 2017, MNRAS, 466, 4272
Dugan Z., Bryan S., Gaibler V., Silk J., Haas M., 2014, ApJ, 796, 113
Dullo B. T. et al., 2021, in press
Dunn R. J. H., Fabian A. C., 2006, MNRAS, 373, 959
Esin A. A., McClintock J. E., Narayan R., 1997, ApJ, 489, 865
Esparza-Arredondo D., Osorio-Clavijo N., González-Martín O., Victoria-Ceballos C., Haro-Corzo S. A. R., Reyes-Amador O. U., López-Sánchez J., Pasetto A., 2020, ApJ, 905, 29
Fabian A. C., 2012, ARA&A, 50, 455
Fabian A. C., Canizares C. R., 1988, Nature, 333, 829
Falcke H., Körding E., Markoff S., 2004, A&A, 414, 895
Falcke H., Nagar N. M., Wilson A. S., Ho L. C., Ulvestad J. S., 2001, in Kaper L., Heuvel E. P. J. V. D., Woudt P. A., eds, Black Holes in Binaries and Galactic Nuclei. Springer-Verlag, Berlin, p. 218
Falcke H., Nagar N. M., Wilson A. S., Ulvestad J. S., 2000, ApJ, 542, 197
Fanti C., Fanti R., de Ruiter H. R., Parma P., 1987, A&AS, 69, 57
Faucher-Giguère C.-A., Quataert E., 2012, MNRAS, 425, 605
Feigelson E. D., Nelson P. I., 1985, ApJ, 293, 192
Fender R. P., 2001, MNRAS, 322, 31
Fender R. P., Belloni T. M., Gallo E., 2004, MNRAS, 355, 1105
Fender R. P., Gallo E., Jonker P. G., 2003, MNRAS, 343, L99
Fender R. P., Homan J., Belloni T. M., 2009, MNRAS, 396, 1370
Fernández-Ontiveros J. A., Muñoz-Darias T., 2021, MNRAS, 504, 5726
Fernández-Ontiveros J. A., Prieto M. A., Acosta-Pulido J. A., 2009, MNRAS, 392, L16
Ferreira J., 1997, A&A, 319, 340
Ferreira J., Petrucci P. O., Murphy G., Zanni C., Henri G., 2010, Astronomical Society of the Pacific Conference Series. Jet Emitting Discs: a New Accretion Flow Solution. p. 49
Filho M. E., Barthel P. D., Ho L. C., 2006, A&A, 451, 71
Fischer T. C. et al., 2021, ApJ, 906, 88
Flohic H. M. L. G., Eracleous M., Chartas G., Shields J. C., Moran E. C., 2006, ApJ, 647, 140
Forman W., Jones C., Tucker W., 1985, ApJ, 293, 102
Gaibler V., Khochfar S., Krause M., Silk J., 2012, MNRAS, 425, 438
Gallimore J. F., Axon D. J., O'Dea C. P., Baum S. A., Pedlar A., 2006, AJ, 132, 546
Gallo E., Sesana A., 2019, ApJ, 883, L18
Gallo E., Treu T., Jacob J., Woo J.-H., Marshall P. J., Antonucci R., 2008, ApJ, 680, 154
Garofalo D., Bishop K., 2020, PASP, 132, 114103
Garofalo D., Evans D. A., Sambruna R. M., 2010, MNRAS, 406, 975
Garofalo D., Kim M. I., Christian D. J., 2014, MNRAS, 442, 3097
Garofalo D., Singh C. B., 2019, ApJ, 871, 259
Gebhardt K. et al., 2000, ApJ, 539, L13
Giannios D., Metzger B. D., 2011, MNRAS, 416, 2102
Giovannini G., 2003, New A Rev., 47, 551
Giovannini G., 2004, Ap&SS, 293, 1
Giovannini G., Taylor G. B., Feretti L., Cotton W. D., Lara L., Venturi T., 2005, ApJ, 618, 635
Giroletti M., Panessa F., 2009, ApJ, 706, L260
González-Martín O., Masegosa J., Márquez I., Guerrero M. A., Dultzin-Hacyan D., 2006, A&A, 460, 45
Grandi P., Torresi E., Macconi D., Boccardi B., Capetti A., 2021, ApJ, 911, 17
Greene J. E., 2012, Nature Commun., 3, 1304
Greene J. E., Ho L. C., 2007, ApJ, 667, 131
Greene J. E., Strader J., Ho L. C., 2020, ARA&A, 58, 257
Gültekin K., King A. L., Cackett E. M., Nyland K., Miller J. M., Di Matteo T., Markoff S., Rupen M. P., 2019, ApJ, 871, 80
Gürkan G. et al., 2015, MNRAS, 452, 3776
Gürkan G. et al., 2018, MNRAS, 475, 3010
Hardcastle M. J. et al., 2019, A&A, 622, A12
Hardcastle M., 2018, Nature Astron., 2, 273
Hardcastle M., Croston J., 2020, New Astron. Rev., 88, 101539
Häring N., Rix H.-W., 2004, ApJ, 604, L89
Heckman T. M., 1980, A&A, 500, 187
Heckman T. M., Alexandroff R. M., Borthakur S., Overzier R., Leitherer C., 2015, ApJ, 809, 147
Heckman T. M., Best P. N., 2014, ARA&A, 52, 589
Heckman T. M., Kauffmann G., Brinchmann J., Charlot S., Tremonti C., White S. D. M., 2004, ApJ, 613, 109
Heckman T. M., Lehnert M. D., Armus L., 1993, in Shull J. M., Thronson H. A., eds, Astrophysics and Space Science Library, Vol. 188, The Environment and Evolution of Galaxies. Kluwer, Dordrecht, p. 455
Heinz S., Merloni A., Schwab J., 2007, ApJ, 658, L9
Heinz S., Sunyaev R. A., 2003, MNRAS, 343, L59
Herpich F., Stasińska G., Mateus A., Vale Asari N., Cid Fernandes R., 2018, MNRAS, 481, 1774
Heywood I. et al., 2019, Nature, 573, 235
Ho L. C., 1999, ApJ, 516, 672
Ho L. C., 2002, ApJ, 564, 120
Ho L. C., 2008, ARA&A, 46, 475
Ho L. C., Filippenko A. V., Sargent W. L. W., 1997a, ApJS, 112, 315
Ho L. C., Filippenko A. V., Sargent W. L. W., 1997b, ApJ, 487, 568
Ho L. C., Filippenko A. V., Sargent W. L., 1995, ApJS, 98, 477
Ho L. C., Greene J. E., Filippenko A. V., Sargent W. L. W., 2009, ApJS, 183, 1
Ho L. C., Ulvestad J. S., 2001, ApJS, 133, 77
Huchra J., Burg R., 1992, ApJ, 393, 90
Inayoshi K., Ichikawa K., Ho L. C., 2020, ApJ, 894, 141
Ishibashi W., Auger M. W., Zhang D., Fabian A. C., 2014, MNRAS, 443, 1339
Janssen R. M. J., Röttgering H. J. A., Best P. N., Brinchmann J., 2012, A&A, 541, A62
Jarvis M. E. et al., 2019, MNRAS, 485, 2710
Jarvis M. E. et al., 2021, MNRAS, 503, 1780
Jiang L., Fan X., Ivezić Ž., Richards G. T., Schneider D. P., Strauss M. A., Kelly B. C., 2007, ApJ, 656, 680
Kauffmann G. et al., 2003, MNRAS, 346, 1055
Kauffmann G., Heckman T. M., Best P. N., 2008, MNRAS, 384, 953
Kellermann K. I., Sramek R., Schmidt M., Shaffer D. B., Green R., 1989, AJ, 98, 1195
Kelly B. C., Merloni A., 2012, Adv. Astron., 2012, 970858
Kendall M., 1938, Biometrika, 30, 81
Kennicutt R. C., Jr, 1998, ARA&A, 36, 189
Kewley L. J., Groves B., Kauffmann G., Heckman T., 2006, MNRAS, 372, 961
Kewley L. J., Nicholls D. C., Sutherland R. S., 2019, ARA&A, 57, 511
Kharb P. et al., 2012, AJ, 143, 78
Kharb P., O'Dea C. P., Baum S. A., Colbert E. J. M., Xu C., 2006, ApJ, 652, 177
Kharb P., O'Dea C. P., Baum S. A., Hardcastle M. J., Dicken D., Croston J. H., Mingo B., Noel-Storr J., 2014, MNRAS, 440, 2976
Kharb P., Subramanian S., Vaddi S., Das M., Paragi Z., 2017, ApJ, 846, 12
King A. L. et al., 2011, ApJ, 729, 19
Klindt L., Alexander D. M., Rosario D. J., Lusso E., Fotopoulou S., 2019, MNRAS, 488, 3109

Downloaded from https://academic.oup.com/mnras/article/508/2/2019/6385009 by guest on 03 September 2022

Körding E. G., Fender R. P., Migliari S., 2006, MNRAS, 369, 1451
Körding E. G., Jester S., Fender R., 2008, MNRAS, 383, 277
Kormendy J., Ho L., 2001, in Murdin P., ed., Encyclopedia of Astronomy and Astrophysics, Supermassive Black Holes in Inactive Galaxies. Institute of Physics Publishing, Bristol, p. 2635
Kozieł-Wierzbowska D., Stasińska G., Vale Asari N., Sikora M., Goettems E., Wójtowicz A., 2017, Front. Astron. Space Sci., 4, 39
Kukula M. J., Ghosh T., Pedlar A., Schilizzi R. T., 1999, ApJ, 518, 117
Kukula M. J., Ghosh T., Pedlar A., Schilizzi R. T., Miley G. K., de Bruyn A. G., Saikia D. J., 1993, MNRAS, 264, 893
Kukula M. J., Pedlar A., Baum S. A., O'Dea C. P., 1995, MNRAS, 276, 1262
Lagos C. D. P., Padilla N. D., Cora S. A., 2009, MNRAS, 395, 625
Lamastra A., Bianchi S., Matt G., Perola G. C., Barcons X., Carrera F. J., 2009, A&A, 504, 73
Laor A., 2000, ApJ, 543, L111
Laor A., Baldi R. D., Behar E., 2019, MNRAS, 482, 5513
Laor A., Behar E., 2008, MNRAS, 390, 847
Lapi A. et al., 2011, ApJ, 742, 24
Lavalley M., Isobe T., Feigelson E., 1992, in Worrall D. M., Biemesderfer C., Barnes J., eds, ASP Conf. Ser. Vol. 25, ASURV: Astronomy Survival Analysis Package. Astron. Soc. Pac., San Francisco, p. 245
Liu X., Chang N., Han Z., Wang X., 2020, Universe, 6, 68
Maccarone T. J., 2003, A&A, 409, 697
Macfarlane C. et al., 2021, MNRAS, 506, 5888
Magorrian J. et al., 1998, AJ, 115, 2285
Mancuso C. et al., 2017, ApJ, 842, 95
Maoz D., 2007, MNRAS, 377, 1696
Marconi A., Risaliti G., Gilli R., Hunt L. K., Maiolino R., Salvati M., 2004, MNRAS, 351, 169
Markoff S., Nowak M. A., Wilms J., 2005, ApJ, 635, 1203
Markoff S., Nowak M., Corbel S., Fender R., Falcke H., 2003, New A Rev., 47, 491
Markowitz A. et al., 2003, ApJ, 593, 96
Martín-Navarro I., Mezcua M., 2018, ApJ, 855, L20
Mascoop J. L., Anderson L. D., Wenger T. V., Makai Z., Armentrout W. P., Balser D. S., Bania T. M., 2021, ApJ, 910, 159
Massaglia S., Bodo G., Rossi P., Capetti S., Mignone A., 2016, A&A, 596, A12
Mattila S. et al., 2018, Science, 361, 482
Mauch T., Sadler E. M., 2007, MNRAS, 375, 931
McKinney J. C., Tchekhovskoy A., Blandford R. D., 2012, MNRAS, 423, 3083
Meier D. L., 2001, ApJ, 548, L9
Meier D. L., 2012, Black Hole Astrophysics: The Engine Paradigm. Springer-Verlag, Berlin Heidelberg
Merloni A., Heinz S., 2007, MNRAS, 381, 589
Merloni A., Heinz S., di Matteo T., 2003, MNRAS, 345, 1057
Mezcua M., 2017, Int. J. Mod. Phys. D, 26, 1730021
Mezcua M., Prieto M. A., 2014, ApJ, 787, 62
Middelberg E. et al., 2004, A&A, 417, 925
Mingo B. et al., 2019, MNRAS, 488, 2701
Moderski R., Sikora M., Lasota J. P., 1998, MNRAS, 301, 142
Morganti R., 2017, Frontiers Astron. Space Sci., 4, 42
Morganti R., Fanti C., Fanti R., Parma P., de Ruiter H. R., 1987, A&A, 183, 203
Morganti R., Tsvetanov Z. I., Gallimore J., Allen M. G., 1999, A&AS, 137, 457
Moustakas J., Kennicutt R. C. J., Tremonti C. A., 2006, ApJ, 642, 775
Mukherjee D., Bicknell G. V., Wagner A. Y., Sutherland R. S., Silk J., 2018, MNRAS, 479, 5544
Mukherjee D., Bodo G., Mignone A., Rossi P., Vaidya B., 2020, MNRAS, 499, 681
Mulcahey C. R. et al., 2021, in press
Mundell C. G., Ferruit P., Nagar N., Wilson A. S., 2009, ApJ, 703, 802
Mundell C. G., Wilson A. S., Ulvestad J. S., Roy A. L., 2000, ApJ, 529, 816
Muxlow T. W. B. et al., 2020, MNRAS, 495, 1188
Nagar N. M., Falcke H., Wilson A. S., 2005, A&A, 435, 521
Nagar N. M., Falcke H., Wilson A. S., Ho L. C., 2000, ApJ, 542, 186
Nagar N. M., Falcke H., Wilson A. S., Ulvestad J. S., 2002, A&A, 392, 53
Narayan R., 2005, Ap&SS, 300, 177
Narayan R., McClintock J. E., 2008, New A Rev., 51, 733
Narayan R., Yi I., 1994, ApJ, 428, L13
Narayan R., Yi I., 1995, ApJ, 444, 231
Nelson C. H., 2000, ApJ, 544, L91
Nemmen R. S., Bower R. G., Babul A., Storchi-Bergmann T., 2007, MNRAS, 377, 1652
Nemmen R. S., Storchi-Bergmann T., Eracleous M., 2014, MNRAS, 438, 2804
Netzer H., 2009, MNRAS, 399, 1907
Neumayer N., Seth A., Böker T., 2020, A&A Rev., 28, 4
Nyland K. et al., 2020, ApJ, 905, 74
Padovani P., 2016, A&A Rev., 24, 13
Padovani P., Bonzini M., Kellermann K. I., Miller N., Mainieri V., Tozzi P., 2015, MNRAS, 452, 1263
Panessa F., Baldi R. D., Laor A., Padovani P., Behar E., McHardy I., 2019, Nature Astron., 3, 387
Panessa F., Barcons X., Bassani L., Cappi M., Carrera F. J., Ho L. C., Pellegrini S., 2007, A&A, 467, 519
Panessa F., Bassani L., Cappi M., Dadina M., Barcons X., Carrera F. J., Ho L. C., Iwasawa K., 2006, A&A, 455, 173
Parma P., de Ruiter H. R., Fanti C., Fanti R., 1986, A&AS, 64, 135
Paudel S., Yoon S.-J., 2020, ApJ, 898, L47
Pearson K., 1895, Proc. R. Soc. London Ser. I, 58, 240
Pedlar A., Unger S. W., Dyson J. E., 1985, MNRAS, 214, 463
Perlman E. S., Biretta J. A., Zhou F., Sparks W. B., Macchetto F. D., 1999, AJ, 117, 2185
Pitchford L. K. et al., 2016, MNRAS, 462, 4067
Plotkin R. M., Markoff S., Kelly B. C., Körding E., Anderson S. F., 2012, MNRAS, 419, 267
Radcliffe J. F. et al., 2018, A&A, 619, A48
Raginski I., Laor A., 2016, MNRAS, 459, 2082
Reines A. E., Volonteri M., 2015, ApJ, 813, 82
Remillard R. A., McClintock J. E., 2006, ARA&A, 44, 49
Reynolds C. S., Begelman M. C., 1997, ApJ, 487, L135
Risaliti G., Salvati M., Marconi A., 2011, MNRAS, 411, 2223
Rosario D. J., Fawcett V. A., Klindt L., Alexander D. M., Morabito L. K., Fotopoulou S., Lusso E., Calistro Rivera G., 2020, MNRAS, 494, 3061
Rossi P., Bodo G., Massaglia S., Capetti A., 2020, A&A, 642, A69
Roy N. et al., 2021, ApJ, preprint (arXiv:2109.02609)
Rushton A. et al., 2012, MNRAS, 419, 3194
Rusinek K., Sikora M., Kozieł-Wierzbowska D., Gupta M., 2020, ApJ, 900, 125
Sabater J. et al., 2019, A&A, 622, A17
Saikia P., Körding E., Dibi S., 2018a, MNRAS, 477, 2119
Saikia P., Körding E., Coppejans D. L., Falcke H., Williams D., Baldi R. D., McHardy I., Beswick R., 2018b, A&A, 616, A152
Saikia P., Körding E., Falcke H., 2015, MNRAS, 450, 2317
Salucci P., Szuszkiewicz E., Monaco P., Danese L., 1999, MNRAS, 307, 637
Sandage A., Tammann G. A., 1981, A Revised Shapley-Ames Catalog of Bright Galaxies. Carnegie Institution of Washington, Publ., Washington, p. 635
Santini P. et al., 2012, A&A, 540, A109
Sarzi M. et al., 2010, MNRAS, 402, 2187
Schmitt J. H. M. M., 1985, ApJ, 293, 178
Scott N., Graham A. W., 2013, ApJ, 763, 76
Shakura N. I., Sunyaev R. A., 1973, A&A, 24, 337
Shankar F. et al., 2019, MNRAS, 485, 1278
Shankar F. et al., 2020, Nature Astron., 4, 282
Shankar F., 2009, New A Rev., 53, 57
Shankar F., Salucci P., Granato G. L., De Zotti G., Danese L., 2004, MNRAS, 354, 1020
Silpa S., Kharb P., Ho L. C., Ishwara-Chandra C. H., Jarvis M. E., Harrison C., 2020, MNRAS, 499, 5826
Singh R. et al., 2013, A&A, 558, A43
Singh V., Shastri P., Risaliti G., 2011, A&A, 532, A84
Smith K. L. et al., 2020a, MNRAS, 492, 4216

Downloaded from https://academic.oup.com/mnras/article/508/2/2019/6385009 by guest on 03 September 2022

Smith K. L., Koss M., Mushotzky R., Wong O. I., Shimizu T. T., Ricci C., Ricci F., 2020b, ApJ, 904, 83
Smolčić V. et al., 2008, ApJS, 177, 14
Soltan A., 1982, MNRAS, 200, 115
Speagle J. S., Steinhardt C. L., Capak P. L., Silverman J. D., 2014, ApJS, 214, 15
Suzuki T. L. et al., 2016, MNRAS, 462, 181
Tadhunter C., 2016, A&A Rev., 24, 10
Talbot R. Y., Bourne M. A., Sijacki D., 2021, MNRAS, 504, 3619
Tchekhovskoy A., McKinney J. C., 2012, MNRAS, 423, L55
Tchekhovskoy A., Narayan R., McKinney J. C., 2011, MNRAS, 418, L79
Terashima Y., Iyomoto N., Ho L. C., Ptak A. F., 2002, ApJS, 139, 1
Terashima Y., Wilson A. S., 2003, ApJ, 583, 145
Thean A., Pedlar A., Kukula M. J., Baum S. A., O'Dea C. P., 2000, MNRAS, 314, 573
Tremaine S. et al., 2002, ApJ, 574, 740
Trippe S., 2014, J. Korean Astron. Soc., 47, 159
Ulvestad J. S., Wilson A. S., Sramek R. A., 1981, ApJ, 247, 419
Vahdat Motlagh A., Kalemci E., Maccarone T. J., 2019, MNRAS, 485, 2744
van den Bosch R. C. E., 2016, ApJ, 831, 134
Vaughan S., Iwasawa K., Fabian A. C., Hayashida K., 2005, MNRAS, 356, 524
Venturi G. et al., 2021, A&A, 648, A17
Vitale M., Fuhrmann L., García-Marín M., Eckart A., Zuther J., Hopkins A. M., 2015, A&A, 573, A93
Walker R. C., Romney J. D., Benson J. M., 1994, ApJ, 430, L45
Weaver R., McCray R., Castor J., Shapiro P., Moore R., 1977, ApJ, 218, 377
Webster B. et al., 2021, MNRAS, 500, 4921
Werner N., McNamara B. R., Churazov E., Scannapieco E., 2019, Space Sci. Rev., 215, 5
White C. J., Quataert E., Gammie C. F., 2020, ApJ, 891, 63
Williams D. R. A. et al., 2019, MNRAS, 486, 4962
Williams D. R. A. et al., 2021, in press
Wójtowicz A., Stawarz Ł., Cheung C. C., Ostorero L., Kosmaczewski E., Siemiginowska A., 2020, ApJ, 892, 116
Wrobel J. M., 2000, ApJ, 531, 716
Yang H., Yuan F., Yuan Y.-F., White C. J., 2021, ApJ, 914, 131
Yang X. et al., 2020, ApJ, 904, 200
Yesuf H. M., Faber S. M., Koo D. C., Woo J., Primack J. R., Luo Y., 2020, ApJ, 889, 14
Yi I., Boughn S. P., 1998, ApJ, 499, 198
Yi I., Boughn S. P., 1999, ApJ, 515, 576
Yuan F., Narayan R., 2014, ARA&A, 52, 529
Yuan F., Bu D., Wu M., 2012a, ApJ, 761, 130
Yuan F., Wu M., Bu D., 2012b, ApJ, 761, 129
Zakamska N. L., Greene J. E., 2014, MNRAS, 442, 784

SUPPORTING INFORMATION

Supplementary data are available at *MNRAS* online.

Appendix A. Local Black hole mass function.
Figure A1. Specific star-formation rate (sSFR [yr^{-1}], left *y*-axis) versus M_{BH} ($M_{\odot}$) for star-forming galaxies and the local BHMF (Mpc^{-3} dex^{-1}, right *y*-axis) of active galaxies.
Table 1. Radio and optical properties of the LeMMINGs (Palomar) sample.

Please note: Oxford University Press is not responsible for the content or functionality of any supporting materials supplied by the authors. Any queries (other than missing material) should be directed to the corresponding author for the article.

[1]*Istituto di Radioastronomia, INAF, Via P. Gobetti 101, I-40129 Bologna, Italy*
[2]*School of Physics and Astronomy, University of Southampton, Southampton SO17 1BJ, UK*
[3]*Jodrell Bank Centre for Astrophysics, School of Physics and Astronomy, The University of Manchester, Manchester M13 9PL, UK*
[4]*Departamento de Física de la Tierra y Astrofísica, Instituto de Física de Partículas y del Cosmos IPARCOS, Universidad Complutense de Madrid, E-28040 Madrid, Spain*
[5]*Instituto de Astrofísica de Canarias, Via Láctea S/N, E-38205, La Laguna, Tenerife, Spain*
[6]*Departamento de Astrofísica, Universidad de La Laguna, E-38206, La Laguna, Tenerife, Spain*
[7]*Jeremiah Horrocks Institute, University of Central Lancashire, Preston PR1 2HE, UK*
[8]*Department of Space, Earth and Environment Chalmers University of Technology, SE-412 96 Gothenburg, Sweden*
[9]*Instituto de Astrofisica de Andalucía (IAA, CSIC), Glorieta de la Astronomía s/n, E-18008-Granada, Spain*
[10]*Netherlands Institute for Radio Astronomy, ASTRON, Nl-79901 PD Dwingeloo, The Netherlands*
[11]*UK ALMA Regional Centre Node, Jodrell Bank Centre for Astrophysics, UK*
[12]*Department of Physics & Astronomy, University College London, Gower Street, London WC1E 6BT, UK*
[13]*Astrophysics Group, Cavendish Laboratory, 19 J. J. Thomson Avenue, Cambridge CB3 0HE, UK*
[14]*Max-Planck-Institut für Radioastronomie, Auf dem Hügel 69, D-53121 Bonn, Germany*
[15]*Department of Astrophysics/IMAPP, Radboud University, P.O. Box 9010, NL-6500 GL Nijmegen, The Netherlands*
[16]*Department of Physics, Box 41051, Science Building, Texas Tech University, Lubbock, TX 79409, USA*
[17]*Real Academia de Ciencias, C/ Valverde 22, E-28004 Madrid, Spain*
[18]*Technical University of Kenya, P.O. Box 52428-00200, Nairobi, Kenya*
[19]*INAF, Istituto di Astrofisica e Planetologia Spaziali, via Fosso del Cavaliere 100, I-00133 Roma, Italy*
[20]*Institute of Astronomy and Astrophysics, Academia Sinica, 11F of Astronomy-Mathematics Building, AS/NTU No. 1, Section 4, Roosevelt Rd, Taipei 10617, Taiwan, R.O.C*
[21]*Inter-University Centre for Astronomy and Astrophysics (IUCAA), Ganeshkhind P.O., Pune 411007, India*
[22]*Center for Astro, Particle and Planetary Physics, New York University Abu Dhabi, P.O. Box 129188, Abu Dhabi, UAE*
[23]*School of Physics and Astronomy, University of Birmingham, Edgbaston, Birmingham B15 2TT, UK*
[24]*Anton Pannekoek Institute for Astronomy, University of Amsterdam, Science Park 904, NL-1098 XH Amsterdam, the Netherlands*
[25]*Centre for Astrophysics Research, University of Hertfordshire, College Lane, Hatfield AL10 9AB, UK*
[26]*Station de Radioastronomie de Nançay, Observatoire de Paris, PSL Research University, CNRS, Université Orléans, F-18330 Nançay, France*
[27]*AIM, CEA, CNRS, Université de Paris, Université Paris Saclay, F-91191 Gif-sur-Yvette, France*
[28]*Dpt. Astronomia i Astrofísica, Unversitat de València, C/Dr. Moliner 50, E-46100 Burjassot, Valencia, Spain*
[29]*Department of Physics, University of Bath, Claverton Down, Bath BA2 7AY, UK*
[30]*Department of Physics, Indian Institute of Technology, Hyderabad 502285, India*
[31]*Centre for Extragalactic Astronomy, Department of Physics, Durham University, Durham DH1 3LE, UK*

This paper has been typeset from a TEX/LATEX file prepared by the author.

Downloaded from https://academic.oup.com/mnras/article/508/2/2019/6385009 by guest on 03 September 2022